





LIBRARY Michigan State University

This is to certify that the

thesis entitled

CONTROL OF CONDUCTIVE HEAT TRANSFER
IN ELECTRORHEOLOGICAL FLUID
COMPOSITES

presented by

GLORIA D. ELLIOTT

has been accepted towards fulfillment of the requirements for

M.S. degree in MECHANICAL ENGINEERING

Date APRIL 29, 1997

MSU is an Affirmative Action/Equal Opportunity Institution

O-7639

PLACE IN RETURN BOX to remove this checkout from your record. TO AVOID FINES return on or before date due.

DATE DUE	DATE DUE	DATE DUE

MSU is An Affirmative Action/Equal Opportunity Institution

CONTROL OF CONDUCTIVE HEAT TRANSFER IN ELECTRORHEOLOGICAL FLUID COMPOSITES

By

Gloria D. Elliott

A THESIS

Submitted to
Michigan State University
in partial fulfillment of the requirements
for the degree of

MASTER OF SCIENCE

Department of Mechanical Engineering

ABSTRACT

CONTROL OF CONDUCTIVE HEAT TRANSFER IN ELECTRORHEOLOGICAL FLUID COMPOSITES

By

Gloria D. Elliott

The majority of electrorheological (ER) fluid applications are based on the controllable viscosity changes characteristic of these suspensions. When subjected to high voltage fields the suspended particles experience a charge separation causing them to reorient and to form fibrillar chain structures perpendicular to the electrodes, which in turn induces a change in viscosity of the fluid. Controllable heat transfer is thus possible if the heat transfer properties are similarly affected by electric field strength. A methodology was developed to evaluate the thermal properties of chained electrorheological fluids under such high voltage conditions. Video imaging was implemented to gain a general understanding of the electrorheological response. Thermal conductivity (k) and volumetric specific heat (ρC_p) estimates were obtained in both zero and high DC field conditions using a one-dimensional transient heat conduction model and Prop-1D software. Within the limits imposed by this technique no detectable change in thermal properties was observed.

To my family

Acknowledgments

I'd like to thank my advisor, Dr. John Lloyd, for supervising this work and for allowing me the freedom to explore the aspects of this project that weren't necessarily part of the original strategy. I'd also like to express my appreciation to my committee members Dr. Radcliffe and Dr. Beck, for their helpful advice and discussions during the course of this research. I am also very grateful to Dr. John McGrath for his patience during the completion of this work.

For guiding me in a direction that I have never once regretted, special thanks to Kent Nielsen. To Kohichiro Kawate-san I have to say arigatoo gozaimasu for inciting my enthusiasm for research and for so positively impacting my academic pursuits.

Among my peers, I have to especially thank Mark Wilenski, who took the time to understand my research difficulties and was a fountain of hope when things seemed impossible, and Kevin Dowding, for his never-ending patience in discussing the details of parameter estimation on so many an occasion. Without the support of so many of my colleagues the completion of this thesis would have seemed an impossible task. To my labmates P.T. Ramakrishnan, Xinsue Su, and Jeff Hargrove, I owe special thanks for their helpful discussions and assistance. Many thanks to Heidi Relyea, Paul Hoke, Joe DeRose, Mark Minor, and Charles Birdsong, who so graciously listened to many a monologue, and provided a rally of support during the difficult times.

Finally, I have to thank my family for instilling in me the belief that I could achieve whatever I set out to do.

Table of Contents

LIS	ST OF TABLES	ix
LIS	ST OF FIGURES	x
NO	DMENCLATURE	xiii
1	Introduction	. 1
2	Design and Preparation of Electrorheological Fluids	9
3	Video Imaging of Chaining Response	.14
	3.1 Imaging Apparatus and Technique	. 14
	3.2 Observations	.17
	3.3 Discussion.	. 22
	Determination of Thermal Conductivity and Volumetric	
Sp	ecific Heat using a 1-D Heat Conduction Model	. 25
	4.1 Transient Measurements	. 25
	4.1.1 Overview of Method	25

		4.1.2	Apparatus	and Analytical Technique	27
			4.1.2.1	Composite Specimen	27
			4.1.2.2	Data Acquisition System	33
		4.1.3	Governing	Equations and Boundary Conditions	35
		4.1.4	Data Anal	ysis	36
		4.1.5	Experimen	ntal Method	38
		4.1.6	Results an	d Discussion	38
		4.1.7	Error Ana	lysis	57
	4.2	Steady	-State Mea	surements	58
5	Concl	lusions	and Reco	ommendations	61
A	Funda	amenta	l Issues		65
	A.	l Int	er-particle	Forces	65
	A	2 Die	electric Phe	nomena	69
	A	3 Int	erfacial Ele	ectric Double Layer Theory	75
В	Triple	e Junct	ion Thern	nocouples	7 8
C	Q-Ba	sic Pro	gram for	Temperature Data Conversion	80
D	PROI	P-1D S	ample Da	ta Files	. 81

E	Design o	Experiment 93	3
	E .1	Sensitivity Analysis 93	3
	E.2	Sequential Estimates	6
	E.3	Residuals	8
	E.4	Duration of Experiment 99	9
F	MDSC I	etermination of Specific Heat10	00
	F.1	Modulated Differential Scanning Calorimetry (MDSC) 10	00
	F.2	Results and Discussion	03
		F.2.1 Calibration. 10	03
		F.2.2 Zeolite Type 3A in Silicon Oil	04
		F.2.3 Error Analysis	05
G	An Error	and Sensitivity Analysis10	07
Li	st of Refe	ences10	09

List of Tables

Table 2.1	Physical Properties of ER fluid materials	10
Table 2.2	Estimates of ER fluid densities	11
Table 2.3	Typical ER Fluid Formulations	13
Table 4.1	Material properties of components used in the composite specimen.	33
Table 4.2	Thermal conductivity values for aluminum oxide and silicon dioxide (Gebhart, 1993)	46
Table E.1	Optimal heating and experimental duration	99
Table F.1	Calculation of MDSC calibration constant	103
Table F.2	Calibration check with sapphire	104
Table F.3	Comparison of literature and experimental values of specific heat of silicon oil	104
Table G.1	Measurement error in material dimensions	107
Table G.2	Sensitivity of thermal property estimation to measurement errors	108

List of Figures

Figure 1.1	Polarization of particles and subsequent chain formation along electric field line vectors: (a) particles are electrically neutral (b) charge separation occurs as the field is turned on (c) particles begin to line up positive and negative ends (d) single chains compact into thicker columns.	2
	compact into thicker columns	J
Figure 1.2	Two extremes of particle orientation (Furmanski and Floryan, 1994)	6
Figure 3.1.	Microscopic Imaging Apparatus: acrylic base and stainless steel electrodes.	.14
Figure 3.2	Elecrodes: (a)Sawtooth (b)Stepped	. 15
Figure 3.3	Dynamic Imaging System comprised of high voltage supply/amplifier, light microscope and CCD camera, video caliper, video cassette recorder, and monitor	. 16
Figure 3.4	2% by volume Type 3A zeolite in silicon oil at a field strength of (a)330 V/mm (b)1000 V/mm (c)1700 V/mm	. 17
Figure 3.5	A field strength of 660V /mm had been applied for several minutes. 5 minutes after removal of the field evidence of redistribution was observed	
Figure 3.6	Sawtooth electrodes: The distance between tips and valleys are 1.0 mm and 2.0 mm respectively, giving rise to field strengths between 500 V/mm and 1000 V/mm.	19
Figure 3.7	Stepped electrodes: the separation in the upper section is 4.65 mm and in the lower section, 2.0 mm. (a)Upper Field Strength: 215 V/mm, Lower: 475 V/mm (b) Upper Field Strength:	
	430 V/mm, Lower:950V/mm	. 20

Figure 3.8	ER chaining response in a region of transitioning field strengths. The chaining occurs in accordance with electric field lines	. 21
Figure 3.9	Appearance of bubbles and/or particulate matter at the negative electrode	. 21
Figure 4.1	One-half of the symmetrical composite specimen: a) Teflon air spacer aluminum electrode c) Teflon gasket to contain the ER fluid aluminum electrode.	. 28
Figure 4.2	Triple junction T-type Copper-Constantan thermocouples attached to aluminum electrodes with poly(vinyl)chloride electrical tape backing.	
Figure 4.3	The fully assembled composite specimen.	. 31
Figure 4.4	Model for Prop-1D analysis.	31
Figure 4.5	Data Acquisition System.	. 34
Figure 4.6	Estimates of thermal conductivity of silicon oil	. 39
Figure 4.7	Estimates of volumetric specific heat of silicon oil	. 39
Figure 4.8	Estimates of thermal conductivity of water	. 41
Figure 4.9	Estimates of volumetric specific heat of water	. 42
Figure 4.10	Estimates of the thermal conductivity of 10% volume fraction Type 3A zeolite/ silicon oil	. 43
Figure 4.11	Estimates of the volumetric specific heat of 10% volume fraction type 3A zeolite/silicon oil	. 4 4
Figure 4.12	Estimates of thermal conductivity of a wet and dry series of type 3A zeolite/silicon oil suspensions	. 45
Figure 4.13	Thermal conductivity of f _v = 5% Type 3A zeolite/silicon oil suspension at low field strengths	47
Figure 4.14	Volumetric specific heat of $f_v = 5\%$ Type 3A zeolite/silicon oil suspension at low field strengths	. 48
Figure 4.15	Thermal conductivity of f _v = 10% and 20% Type 3A zeolite/silicon oil suspensions at low field strengths	

Figure 4.16	Volumetric specific heat of $f_v = 10\%$ and 20% Type 3A zeolite/silicon oil suspension at low field strengths
Figure 4.17	Effect of electric field on the temperature distribution in the ER fluid system
Figure 4.18	The temperature profiles measured across the composite specimen as the steady-state condition developed
Figure A.1	Environmental Scanning Electron Microscopy (ESEM) image of UOP Type 3A zeolite in a minimum amount of silicon oil 67
Figure A.2	Conceptualization of a dielectric particle experiencing a charge separation due to an applied electric field E_0 . (a) The centers of positive charge in the dielectric particle (Na^+ ions in zeolites) shift towards the negative electrode, and the centers of negative charge shift towards the positive electrode (b) The result is a net positive surface charge on the one side of the particle and a net negative charge on the other.
Figure A.3	Types of polarization mechanisms observed in non-polar molecules (von Hippel, 1995):(a)electronic (b)atomic (c)orientation.
Figure B.1	Construction of parallel 3 junction thermocouples:(a) typical construction (b)-(d) electrically equivalent constructions based on the Law of Intermediate Metals for thermocouples
Figure E.1	Thermal conductivity sensitivity coefficients
Figure E.2	Volumetric specific heat sensitivity coefficients
Figure E.3	Comparison of measured profiles and those generated using the parameters estimated by Prop-1D
Figure E.4	Sequential estimates of thermal conductivity97
Figure E.5	Sequential estimates of volumetric specific heat
Figure E.6	Residual analysis for silicon oil, X=0 boundary98
Figure E.7	Residual analysis for silicon oil, X=L boundary98
Figure F.1	Values of specific heat for a series of ER fluids

Nomenclature

A	Area	$[\mathbf{m}^2]$
$A_{\mathbf{K}}$	Amplitude of Kinetic Response	[-]
$\mathbf{A}_{\mathbf{T}}$	Amplitude of Temperature Modulation	[-]
C_p	Specific Heat	[kJ/kgK]
E	Voltage	[V]
E	Electric Field	[v]
$\mathbf{E_0}$	Applied External Field	[V/mm]
$\mathbf{E_i}$	Induced Electric Field	[V/mm]
F	Average Field	[V/mm]
G	Free Energy of Attraction	[-]
I	Current	[A]
$K(C_p)$	MDSC Calibration Constant	[-]
L	Length	[m]
P	Period	[s]
P	Polarization	
R	Resistance	[Ω]
T	Temperature	ici
V	Volume	$[m^3]$
ΔΧ	Thickness	[m]
d	Distance	[Angstroms]
f_v	Volume Fraction	[%]
h	Convection Heat Transfer Coefficient	$[W/m^2K]$
k	Thermal Conductivity	[W/mK]
$\mathbf{k_T}$	Thermal Conductivity Ratio	[-]
m	Average Induced Moment	
q	Heat Flux	[W]
r	Nuclei Separation Distance	[Angstroms]
t	Time	[s]
t_q	Duration of Heating	[s]
t_n	Duration of Experiment	[s]

Greek

	GICER	
α	Thermal Diffusivity	$[m^2/s]$
β	Coefficient of Expansion	[m ⁷ /m ³ °C]
8	Depth of a Potential Well	[m/m C]
ε ₀	Relative Permittivity	
K	Dielectric Constant	
μ	Dipole Moment	
ν	Characteristic Frequency	
ρ	Density	$[kg/m^3]$
σ	Conductivity	[Kg/III]
σ_{i}	Induced Surface Charge Density	
ω	Modulation Frequency	
ξ	Linear Heating Rate	[°C/minute]
•	g	[Or minute]
	Italics	
α	Polarizability	
E	Constant Based on Dimensions	
h G	Planck's Constant	[Js]
q	Charge	[e.m.u.]
	Subscripts	
a	Atomic	
c	Composite	
e	Electronic	
f	Fluid	
1	Liquid	
0	Orientational	
p	Particle	
s T	Solid Total	
eff	Effective	
ref	Reference	
	Superscripts	
+	Dimensionless	
att	Attraction	
rep	Repulsion	

Chapter 1

Introduction

W.M. Winslow (1947) was the first to be awarded a patent for the class of fluids he called electroviscous fluids or electro-fluids. However, theories on the viscoelectric phenomena characteristic of these fluids date back to the 19th century (Quinke, 1897; Duff, 1896). The distinguishing feature of electro-fluids is a viscosity controllable by the application of a high voltage electric field. Winslow (1949) observed a marked increase in flow resistance when these fluids were subjected to electric fields of the order 2-4 kV/mm and attributed this response to an increase in viscosity. In static systems he observed that the application of such fields caused solidification of the fluid, requiring a force proportional to the square of the electric field to shear the material.

Winslow's electroviscous fluids were later renamed electrorheological (ER) fluids by Stangroom (1983) who felt that classifying this induced shear resistance as a viscous response was too stringent. The non-Newtonian behavior of Winslow's fluids could not be explained strictly in terms of viscosity. More encompassing of this phenomena, and better representing the fluid's behavior, was the term 'electrorheological'.

Electrorheological (ER) fluids are typically defined as being dispersions of finely divided, highly polarizable, solid dielectric particles, in hydrophobic liquid carriers of lower dielectric constant (Halsey, 1992). When subjected to a high voltage field, the particles become polarized. The positive and negative charge densities shift to opposite ends of the particle, resulting in a net dipole moment. Dipole-dipole attractive forces cause the particles to rotate and translate, aligning positive and negative ends, to form chains of single particle width oriented parallel to the electric field lines. With time, and/or increasing field strength these single chains collapse into thicker, tighter chains, eventually reaching what has been suggested by Tao and Sun (1991a, 1991b) to be a body-centered tetragonal ground state lattice structure. The result is a dramatic transition from an isotropic suspension to a fibrillar anisotropic material with significantly altered material properties. These transitional stages are depicted in Figure 1.1.

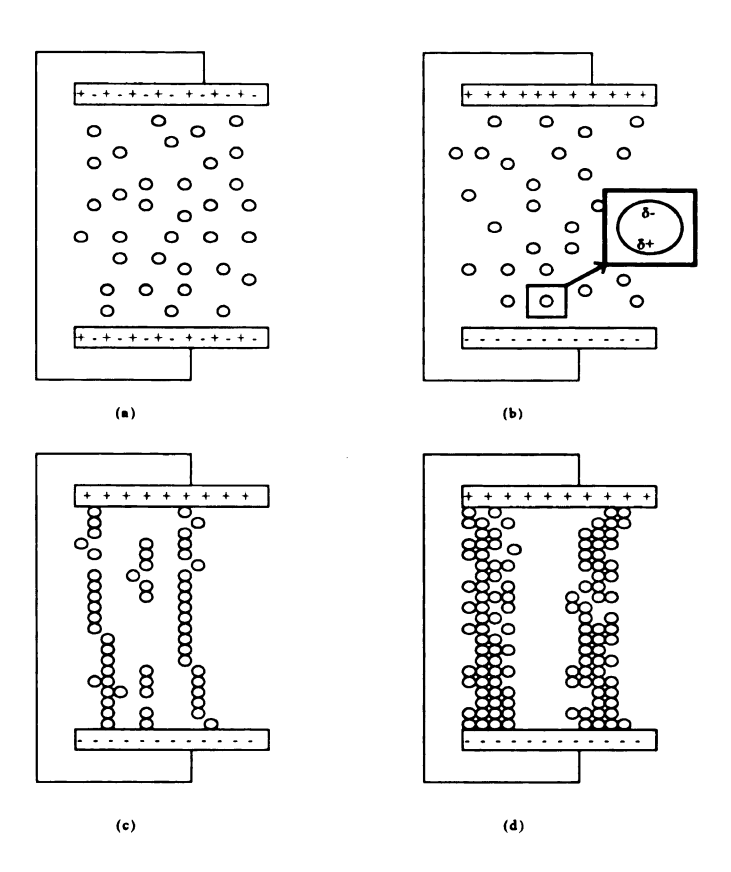


Figure 1.1 Polarization of particles and subsequent chain formation along electric field line vectors: (a) particles are electrically neutral (b) charge separation occurs as the field is turned on (c) particles begin to line up positive and negative ends (d) single chains compact into thicker columns.

Typical field strengths required for activation range from a few hundred volts per mm to upwards of 10 kV/mm, depending on the application, apparatus design, and whether or not the fluid is flowing or static. Removal of the high voltage field causes the dipole-dipole forces to relax thus allowing fluid motion to redistribute the particles.

Several decades after this discovery researchers began to look at the fundamental principles behind the ER response. In 1962 Schwarz proposed an electric double layer theory to account for the dielectric distribution occurring in colloidal dispersions as a result of applied electric fields. Klass and Martinek (1967b) and Uejima (1972)

experimentally supported Schwarz' theory with measurements of dielectric properties of ER fluids, and proposed a dielectric mechanism to explain the Winslow effect.

The 1970's saw a surge in application-oriented research, directed towards harnessing this controllable change in viscosity. The devices proposed by Winslow (1949), a soft-clutch and an electrically controlled valve with no moving parts, were compended by dampers (Eige, 1963), and vibration and shock absorbers (Bullough and Stringer, 1973). Also the first work was done in the area of heat transfer (Shul'man et al., 1977 (in Russian), 1978). Shul'man (1982, 1986) was credited with the first thermal engineering application: the utilization of ER suspensions as the working fluid in heat exchangers. In the same work Shul'man used a transient technique to measure the thermal conductivity of these suspensions in order to improve heat exchanger performance. He found that specific heat (C_n) was insensitive to application of electric fields but suggested that the thermal conductivity (k) could change by upwards of 300% depending on the volume fraction and water-loading of the solid phase. Details of actual thermal Demchuk and Korobko (1977{in conductivity measurements were not included. Russian)) reported thermal conductivity changes up to 280% in suspensions of 5% silica in transformer oil due to application of an electric field, however details of the experimentation were not explicit.

An escalation of mathematical modeling and computational simulations pervaded the next two decades. Adriani and Gast (1988) developed a computational microscopic model of electrorheology, relating microscopic structural changes to macroscopic electrorheological properties. Computer simulations were used by Klingenberg et al. (1989) and Hass (1993) to explore structure formation in electrorheological fluids. Davis

(1992b) was the first to use finite-element analysis to model particle-particle forces in ER fluids.

The 1990's saw a continuation and diversification of heat transfer research. Cha et al. (1990) measured ER fluid density and specific heat as functions of temperature and field strength, observing that within the limits of the experimental technique (0.5%), density was unaffected by field strength. They also observed that the specific heat was insensitive to temperatures less than 100 °C. Zhang & Lloyd (1992) demonstrated that radiation heat transfer through an ER fluid-filled composite window could be controlled by the application of an electric field, and was sensitive to particle concentration and electric field intensity. A 55% increase in thermal conductivity was also reported by Zhang and Lloyd (1993). Alternating current fields were utilized in that work. Lloyd & Zhang (1994) determined effective values of thermal conductivity for both isotropic and chained ER fluids, and compared predicted and experimental values to elucidate the nature of the enhanced heat transfer.

Furmanski and Floryan (1994, 1995) have also been working on adaptive heat transfer systems. Their systems differ in terms of the micro-structural response. The system consists of suspensions of rod-like particles in suitable carrier fluids. These particles transition from an orientation parallel to the wall to a perpendicular orientation when subjected to magnetic or electric fields. This response is depicted in Figure 1.2.

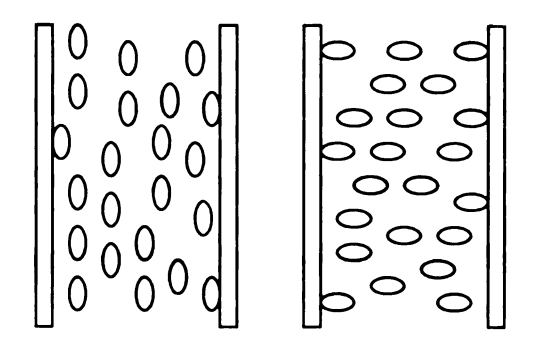


Figure 1.2 Two extremes of particle orientation (Furmanski et. al., 1994).

What has been learned from these systems can be utilized to improve upon the design of electrorheological fluids for heat transfer enhancement because the underlying principles are the same. Furmanski and Floryan (1994) have shown that the heat transfer effects of reorientation are more pronounced when the aspect ratios (length/diameter) of the suspended particles are high.

Concurrent with the developments in the measurement of thermal conductivity were continued efforts to understand the nature of electrical conduction, and its influence on properties. Conrad et al. (1991) concluded that the temperature dependence of the electrical conductivity in zeolite/silicon oil suspensions reflected the diffusion of sodium ions in the zeolite cages. This is consistent with the postulated role of proton mobility (Makatun et al., 1983) in the polarization and conductivity of ER suspensions, based on the results of shearing stress and conductivity experiments.

The present decade has been marked by a renewed interest in dielectric properties.

Conrad et al. (1991) modeled mechanical response in terms of the dielectric mismatch between particle and suspending vehicle and the local field concentration. In an examination of polymer and cellulose derivative-based suspensions, Kordonsky et al.

(1991) demonstrated an increase in molecular mobility and polarizability of the molecules with increasing field intensity due to the addition of functional ionogenic groups (amino, acetyl, phosphate, and others) to the base cellulose. These groups served to increase the proton conductance and thus change the mechanism of electrical conductivity, resulting in an increased rheological sensitivity. An increase in dielectric constant and dielectric loss tangent were thus manifestations of this increased mobility. Conjoint with these observations was an electrorheological dependence on the moisture content of the filler/salt combinations. The resulting surface charge distribution and surface structure due to adsorbed water and its ensuing effect on the electric double layer, positively enhanced the characteristic structure formation in the ER fluids.

As the realization is made that a comprehensive understanding of electrorheological phenomena is only possible with a merging of such areas as physical chemistry, colloid science, electrochemistry, dielectric physics, and interface science, research efforts are becoming much more interdisciplinary in nature. As pointed out by Khusid (1996), computer simulations, which incorporate disperse phase architecture and implement electrostatic models of dielectric property dependences, although qualitatively correct, do not always agree with experimental data. To fully grasp the complex nature of the structure formation in ER fluids and to be able to predict material properties and engineer suspensions with the desired electrical, mechanical, and thermal responses, a continued multi-disciplinary approach is imperative.

The focus of the present work was two-fold. The primary goal was to develop a method of evaluating k and ρC_p of ER fluids when subjected to high voltage fields. Conventional methods of evaluating these properties inhibit the application of high voltage

fields and as such impede property evaluation of ER Fluids in the chained state. Knowledge of the thermal property changes as a function of field strength, particle concentration, moisture content, dielectric properties, etc. provides the basis for the development of thermally smart composites, or materials that can achieve and maintain desired heat transfer properties via open- and closed-loop control. One-dimensional transient and steady-state techniques, combined with a specially designed and modified apparatus, were evaluated for their potential in estimating k and ρC_p of ER fluids in high voltage environments.

Secondly, to be able to design ER fluids with desired controllable thermal responses it is important to understand the fundamental basis of ER phenomena. Thus an equally important aspect of thermal composite design involves developing an understanding of microscopic phenomena, and relating this knowledge to macroscopic observations to elucidate the heat transfer characteristics of ER fluids. Efforts were thus directed towards an investigation into the fundamental science of electrorheological response for the purposes of designing suspensions with controllable thermal properties.

Chapter 2

Design and Preparation of Electrorheological Fluids

The material characteristics proposed by Winslow (1949) to be most suitable for ER activity are still quite applicable today. It was his observation that semi-conductive particles of high dielectric constant tended to yield a strong ER response and that hydrophilic adsorbent materials with nominal degrees of water-loading were especially reactive. Later in his patent on ER fluid compositions (1962) he elaborated on these qualities, indicating that the suspending vehicle should be oleaginous (oily) in nature, have a viscosity in the range of 2 to 20 centipoise at 25 °C, a dielectric constant between 2 and 5.5, and be stable as an electrical insulator (i.e. high dielectric strength). Khusid (1996) has written a more current detailed review of the variety of materials that are being utilized as ER constituents, as well as the nature of their reactivity.

As previously indicated, the choice of constituents will depend on the final application as well as the nature of the electric field being utilized. At the onset of this work the type of field was not considered in the context of choice of materials. The constituents chosen were done so mainly on the basis of Winslow's (1949) observations on appropriate materials. Enhancement of the ER response based on electrical conductivity or dielectric

properties was not considered to be of primary importance. The focus was more on the thermal conductivities of the individual phases.

Type 3A Zeolite, a molecular sieve obtained from Advanced Specialty Gas Equipment, was used as the suspended phase in the electrorheological fluid investigated in this study. The structure of this material is discussed in Appendix A. Dow Corning® Fluid 710, poly(phenyl) siloxane oil, was chosen as the suspending medium. There was convincing evidence in the literature of strong ER response in these materials (Conrad et al., 1994). Type 3A zeolite and silicon oil have similar densities, which aids in preventing settling, a quality not desired in ER fluid composite applications. The physical properties of these materials are given below in Table 2.1.

	Type 3A Zeolite	Silicon Oil
Thermal Conductivity (W/mK)	0.0403 ¹	0.1407
Electrical Conductivity (1/ohm-cm)	$(1 \times 10^{-9} - 1 \times 10^{-12})^2$	1 x 10 ⁻¹³
Density (g/cc)	dry: 1.57 wet: 2.03	1.11
Specific Heat (kJ/kg K)	-	5.99

Table 2.1 Physical Properties of ER fluid materials.

Assuming that the enhanced heat transfer previously observed for ER fluids was directly related to the physical microstructure change as the particles chained up, it was theorized that one phase must dominate in its contribution to the effective thermal conductivity in the anisotropic state. Hence the change in thermal conductivity due to application of an electric field should be optimal when the thermal conductivity values of

-

¹ Zhang and Lloyd, 1993

² Hao and Zu, 1996

the particle and suspending medium are very different. The particle to liquid thermal conductivity ratio in this system is:

$$k_T = \frac{k_p}{k_1} = \frac{0.0403}{0.1407} = 0.2864$$
 [2.1]

This should ensure detectable changes in thermal conductivity as the fluid transitions from isotropic to anisotropic in character.

Samples were prepared in weight fractions according to:

$$f_{v} = \frac{V_{p}}{V_{1}} = \frac{\left(m \rho\right)_{p}}{\left(m \rho\right)_{1}}$$
 [2.2]

where V_p and V_1 are the volumes of particle and fluid, respectively, m the mass, and ρ the density. The zeolite density used for these calculations was 1.80 g/cc, a value intermediate to the wet and dry densities listed by the manufacturer.

Approximate ER fluid density measurements were made for several different volume fractions. The mass of one cubic centimeter of zeolite suspension was measured and recorded. This was then converted to a density reading in kg/m³. The values determined are given below. Because of the degree of error associated with such measurements, this information is used only in a qualitative manner.

	Wet (g/∞)	Dry (g/∞)
5%	1.18	1.13
10%	-	1.25

Table 2.2 Estimates of ER fluid densities.

The zeolite particles were shipped in an anhydrous state (< 2.5 % wt). It has been demonstrated elsewhere that ER response in zeolite/silicon suspensions is very dependent on moisture content (Uejima, 1972). The laboratory environment was such that control of moisture was very difficult. However, for the most part zeolite crystals placed in an open container and left to equilibrate at ambient temperature and humidity overnight, afforded crystals with satisfactory ER behavior. The ambient relative humidity was measured at the time of fluid preparation using an Omega sling psychrometer. Conditions varied from extremes of 29 % to 60% relative humidity. According to manufacturer's specifications, water adsorption increases rapidly with relative humidity to a saturation value equivalent to the maximum loading capacity of the particles (23% for Type 3A zeolite powder). In the ranges given above, the zeolite particles should be fully water loaded at the time of preparation of the ER fluids.

In an attempt to obtain samples of the extremes of water-loading, pseudo-dry and wet dispersion protocol development was initiated. Wet ER samples were prepared by placing the dry zeolite crystals in a humid environment which had been created by placing a 500 mL beaker of boiling water inside of an inverted 10 L beaker. Although normal room humidity conditions would typically substantiate full water loading, an invariant protocol is preferable.

The dry dispersions were much more challenging to prepare. Although the zeolite crystals were shipped in a dehydrated state, repeated openings of the container invalidated the listed moisture content. The zeolite powder was placed on a watch glass and dried in a 200°C oven for 2 hours. It is acknowledged that this does not dry the crystals completely. The ER dispersions were prepared immediately upon removal from the oven.

To prepare fully anhydrous suspensions, both particle and suspending medium would have to be dried. Also the particles would have to be dried under vacuum and immersed in an anhydrous/hydrophobic suspending medium before removal from the oven to prevent moisture pick-up from the atmosphere upon removal.

The ER fluid suspensions were prepared in volume fractions according to the calculation given in equation 2.2. The appropriate amount of silicon oil was weighed into a small plastic jar. The zeolite crystals were then weighed and transferred into this jar and dispersed using a magnetic stirrer and stir bar. Typical ER fluid formulations are listed below in Table 2.3.

ER fluid (vol. %)	mass zeolite (g)	mass silicon oil (g)
5	0.555	18.05
15	1.667	18.05
20	2.222	18.05

Table 2.3 Typical ER Fluid Formulations.

There are obvious drawbacks to preparation of fluids without more stringent control, reproducibility being the most critical. To prevent this from causing problems in the evaluation of the measuring technique, master batches were prepared to ensure consistency among subsequent tests. Magnetic stirring was implemented to redistribute particles before utilization of the fluid in the test apparatus. The apparatus was not filled until just prior to experimentation to prevent misleading results due to particle settling.

Chapter 3

Video Imaging of Chaining Response

3.1 Imaging Apparatus and Technique

A video imaging system was constructed to record the chaining sequence in ER fluids from initial polarization of particles to the evolution of columnar structures. The electrode system used to induce the ER chaining is shown in Figure 3.1.

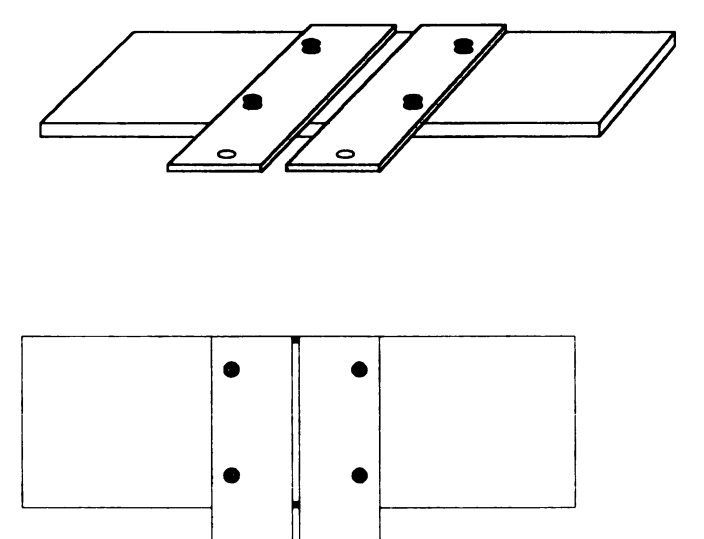


Figure 3.1. Microscopic Imaging Apparatus: acrylic base and stainless steel electrodes.

An acrylic base was cut to the dimensions of a typical glass microscope slide and 1.27 mm stainless steel electrodes were manufactured using wire EDM. Silicon rubber inserts were used to contain the ER fluid between the electrodes. A glass cover slip was placed over the fluid to prevent a meniscus from forming between the electrodes, thus ensuring that the entire surface was in focus at a given time. A drop of Cargille certified refractive index matching fluid with an index of refraction of 1.530 was placed on the cover slip to enhance the optical clarity of the images obtained. Positive and negative leads of a Trek Model 677A supply/amplifier were attached to the electrodes. The magnitude of the applied voltage field was controlled from the front panel of the supply/amplifier. The maximum output voltage of this supply was 2000 V.

The microscopic imaging assembly was modular in design, thus allowing for easy replacement of electrodes. Three electrode geometries were investigated to evaluate the effects of field strength and electric field line density on the chaining mechanisms. These are shown in Figure 3.2.

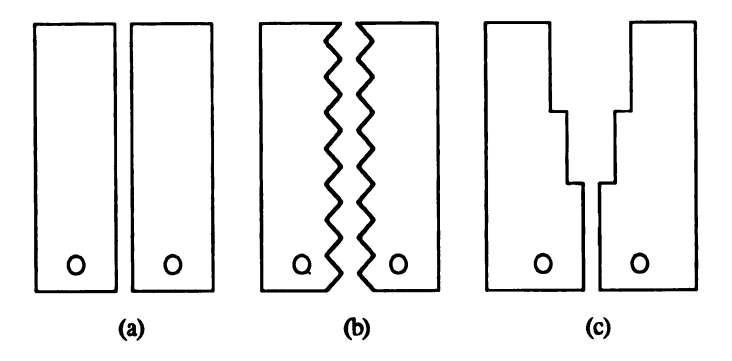


Figure 3.2 Electrodes: (a) Uniform-Gap (b)Sawtooth (b)Stepped

The image acquisition system is depicted schematically in Figure 3.3. A Panasonic WV-CD 20 Charge-Coupled Device (CCD) camera was mounted to an Olympus BH-2 light microscope. The signal from the camera was sent to an Olympus Corp. Cue Micro 300 Video Caliper, and the output from the caliper was then recorded on broadcast quality VHS tape by a Sony video cassette recorder, and displayed on a Sony RGB monitor. Individual images were captured from the video tape for later analysis by using a Data Translations 2625 arithmetic frame grabber board.

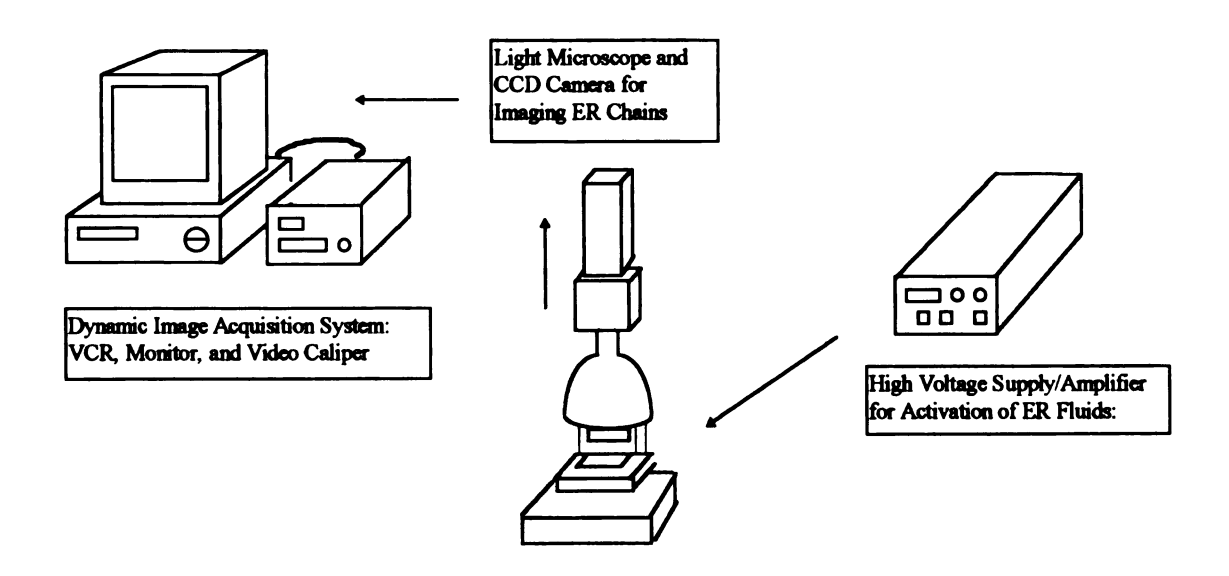


Figure 3.3 Dynamic Imaging System comprised of high voltage supply/amplifier, light microscope and CCD camera, video caliper, video cassette recorder, and monitor.

3.2 Observations

Suspensions of 2% by volume, roughly 1 micron diameter, type 3A zeolite powder in silicon oil were used in the imaging work and provided the best visualization of ER chaining activity. This particular suspension had been prepared at a relative room humidity of 26%. Images of the chaining structure obtained at varying field strengths are shown in Figure 3.4 (a) through (c). From left to right the fields are 330 V/mm, 1000 V/mm, and 1700 V/mm. It can be seen from these images that with increasing field strengths the chain structure becomes thicker.

The time to evolution of full chain structure was found to decrease with increasing field strength. The chain structure at 330 V/mm (Figure 3.4(a)) took upwards of 30 seconds to establish itself whereas the structure at 100V/mm (Figure 3.4(b)) took only 5 or 6 seconds. The time to form the structure at 1700 V/mm (Figure 3.4(c)) was too short to estimate by direct observation.

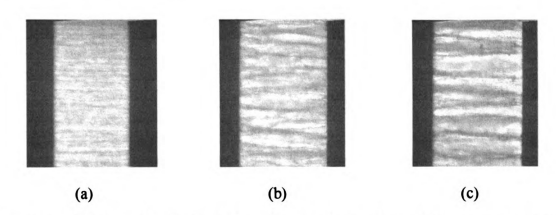


Figure 3.4 2% by volume Type 3A zeolite in silicon oil at a field strength of (a) 330V/mm (b) 1000V/mm (c) 1700 V/mm.

To examine the redistribution of chain structures after field removal, a moderate field strength of 660 V/mm was applied to the sample for several minutes, and then the field level was manually decreased to zero by adjusting the front panel gain. This ensured zero charge on the electrode surfaces. Redistribution occurred but was extremely slow. Previous experiments indicated that return to the fully dispersed state required upwards of 4 to 5 hours and depended on the intensity of the field applied. Redistribution is believed to be caused by Brownian motion. As can be seen in Figure 3.5, after 5 minutes there was still strong evidence of the chaining structure. Sections of the chains were still intact. Reapplication of the 660 V/mm field caused the particles to rapidly snap back into place. Application of higher field strengths caused the chain structures to be locked in upon removal of the field, requiring manual deformation to cause redistribution.

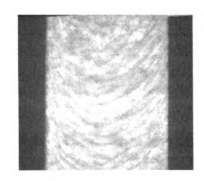


Figure 3.5 A field strength of 660V /mm had been applied for several minutes. 5 minutes after removal of the field evidence of redistribution was observed.

Sawtooth electrodes were used to investigate the effect of electric field line distribution on the ER response. Application of a 1000V field between the electrodes created field strengths between 500V/mm and 1000V/mm. As shown in Figure 3.6, the chaining occurred in a manner consistent with electric field line densities. The ER fluid preferentially chained in the regions of higher field line density, predominantly between the tips of the sawtooth. The chains became thinner and more disperse in the regions where the electric field lines fanned out to areas of lower field line density.

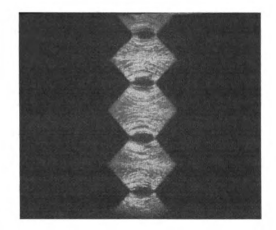


Figure 3.6 Sawtooth electrodes: The distance between tips and valleys are 1.0 mm and 2.0 mm respectively, giving rise to field strengths between 500 V/mm and 1000 V/mm

Figure 3.7 shows the stepped electrode apparatus shown in Figure 3.2 (c) for simultaneous visualization of the effects of two different field strengths. The distance between electrodes in the upper portion is 4.65 mm, whereas in the lower portion the separation is 2.1 mm. In Figure 3.7 (a) in the lower portion of the apparatus the field strength is 475 V/mm, and substantial chaining is observed, whereas in the upper portion

where the field strength is 215 V/mm, there is little evidence of chaining activity. In Figure 3.7 (b) the applied field was increased to 2000V creating a field strength of 430 V/mm in the upper region and 950V/mm in the lower region. Definite chaining was observed in both the upper and lower regions of the apparatus. The field strength for creating observable chaining of this particular fluid under the described conditions was thus somewhere between 215 V/mm and 430 V/mm.

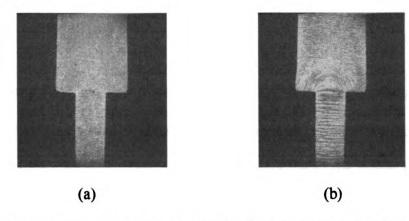


Figure 3.7 Stepped electrodes: The separation in the upper section is 4.65 mm and in the lower section, 2.0 mm. (a)Upper Field Strength:215 V/mm, Lower: 475 V/mm (b) Upper Field Strength:430 V/mm, Lower:950 V/mm

Shown in Figure 3.8 is a close-up of the corner region shown in Figure 3.7. It illustrates the dynamics of the chaining as it bends around the corner in accordance with the electric field lines

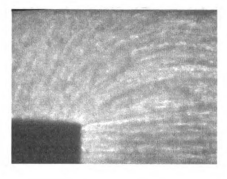


Figure 3.8 ER chaining response in a region of transitioning field strengths. The chaining occurs in accordance with electric field lines.

When the field strength in the straight 1.2 mm gap electrode apparatus was increased to 1700 V/mm, small bubbles or possibly particulate matter were observed at the site of the negative electrode. This became more pronounced the longer the duration of the applied field.



Figure 3.9 Appearance of bubbles and/or particulate matter at the negative electrode.

It is important to note that the field strengths utilized in this work are substantially lower than any of those reported in the literature as typical field strengths applied to induce chaining.

3.3 Discussion

In some systems electrophoresis can be a problem (Monkman, 1991), wherein the particles in the fluid are preferentially attracted to one electrode and repelled from the other. The appearance of this phenomenon on a microscopic level would be a coating of particles on one electrode, with an absence of the same behavior on the other. Near-wall effects such as these can be detrimental in various applications, and can cause complications for most ER fluid modeling work. Such phenomena could potentially be observed, characterized and controlled using microscopic imaging techniques.

Another phenomena that can be calamitous to ER fluid applications is the occurrence of electrolytic reactions in the ER assemblies. Application of direct current fields can precipitate electrolysis reactions, where non-spontaneous chemical reactions occur due the presence of electric currents (Harris, 1987). Water is especially sensitive to electrolysis as can be seen from its reduction and oxidation potentials (Brown et. al., 1991):

$$2(2H_2O(1) + 2e^{-} \Rightarrow H_2(g) + 2OH(aq)) \qquad E^{\circ}_{red} = -0.83 \text{ V}$$

$$2H_2O(1) \Rightarrow 4H^{+}(aq) + O_2(g) + 4e^{-} \qquad E^{\circ}_{ox} = -1.23 \text{ V}$$

$$6H_2O(1) \Rightarrow 4H^{+}(aq) + 4OH(aq) + O_2(g) + 2H_2(g) \qquad E^{\circ}_{cell} = -2.06 \text{ V}$$

Evidence of electrolysis has been seen for the current ER fluid within the stainless steel electrode micro-imaging assembly. Water is the activating species in the ER fluid in this study and is present in significant quantities. An example of this phenomenon is shown in Figure 3.9.

A similar phenomenon was observed with aluminum electrodes as well. The bubbles always appeared at the negative electrode. This seems to be consistent with the reduction of water molecules to produce hydrogen gas bubbles. If the only electrochemical reaction occurring was the electrolysis of water, with time we would expect to see bubbles forming at the positive electrode due to the oxidation of water to produce oxygen gas. This would occur after the reduction because of the relative oxidation and reduction potentials of the two reactions. Instead, a silvery white deposit was seen to accumulate on the positive electrode. It is possible that this corresponds to the reaction of the electrode's aluminum oxide coating with the hydroxide ions produced by the reduction of water at the anode (Brady and Holum, 1993). This reaction is given by:

$$Al_2O_3(s) + 2OH^{-}(aq) + 7H_2O \Rightarrow 2[Al(H_2O)_2(OH)_4]^{-}(aq)$$

Such a coating should revert back to aluminum oxide with heating, however this was not observed to be the case. Heating with a Meker burner flame did not disrupt the coating. Alternately the white material could be solid sodium forming from the sodium ions in the zeolite cages however this seems unlikely as the reduction potential for sodium ion is greater than that for water, hence water oxidation should occur before this would occur.

$$Na^{+}(aq) + e^{-} \Rightarrow Na(s)$$
 $E^{\circ}_{red} = -2.71 \text{ V}$

Also heating would ionize the sodium, and this was not observed.

From the video imaging it also appears that particulate matter is breaking away from the surface of the electrode. This could be an electrochemical reaction in and of itself or else a product of erosion due to the hydrogen gas generation. If this problem persists it would be informative to further characterize the deposited material and quantify the electrolysis to aid in the redesign of the apparatus to prevent such electrode deterioration.

A critical field strength for this type of breakdown was observed with each individual fluid that was manufactured. For the fluid in this particular study this critical field strength was around 1500 V/mm. In other zeolite/ silicon oil suspensions it has been found to be as low as 500 V/mm. The critical field strength appeared to decrease with increasing water-loading of the zeolite fraction. This seems consistent with the corresponding current increases that arise as a function of increasing water content. This relationship will be discussed in later chapters. According to Faraday's Law of Electrolysis (Whitten et al., 1992) "the amount of substance that undergoes oxidation or reduction at each electrode is directly proportional to the amount of electricity passing through the cell". This is consistent with the observation that further increasing the voltage beyond the critical field strength elicits the first appearance of bubbles in the system, thus rapidly increasing the deterioration process.

Chapter 4

Determination of Thermal Conductivity and Volumetric Specific Heat using a 1-D Heat Conduction Model

4.1 Transient Measurements

4.1.1 Overview of Method

Although there exists a variety of methods for evaluation of thermal conductivity, including absolute axial heat flow or thermal potentiometry, flash diffusivity with infrared thermography, and comparative methods (Rowe, 1995), few of these lend themselves to applicability in high voltage environments. The current work utilized a one-dimensional heat flow apparatus, combined with parameter estimation techniques to evaluate thermal properties. This approach falls under the classification of inverse heat conduction problems (IHCP), an area pioneered by Beck (1962) and Stolz (1960) wherein surface characteristics or properties are estimated from internal temperature measurements. The experimental apparatus typical of this method allows for the insertion of electrodes into the composite specimen, thus permitting the application of high voltage fields necessary for chaining activity.

The inverse heat conduction problem is analytically more difficult to solve than the direct problem. In solving the direct problem, knowledge of heat flux or temperature

histories at the surface of a sample, as well as the material's thermal properties allow for evaluation of internal temperature distributions. The inverse problem involves extraction of the thermal properties, utilizing discrete measurements of the dependent variable and knowledge of the initial and boundary conditions. The analytical solutions for these problems are typically very detailed and typically require the use of Green's functions (Beck et al., 1985).

Parameter estimation is a multi-disciplinary field that utilizes statistical tools to efficiently maximize data used for the estimation of constants and functions in mathematical models (Beck and Arnold, 1977). An evaluation of sensitivity coefficients, residuals, and sequential estimates aid in the redesign of experiments to give optimal precision and accuracy of estimates. Parameter estimation techniques are thus intrinsically related to the solution of inverse heat conduction problems.

To determine thermal properties using parameter estimation techniques, a solvable mathematical model is required, and also a well-designed experiment to extract temperature data. Minimization of a sum of squares function with respect to the unknown parameters will then elicit the desired parameters.

This work utilizes Prop-1D, a program developed by Beck (1989) for analysis of one-dimensional heat conduction problems. The program utilizes minimum confidence regions as the basis for the design of experiments yielding minimum variance estimators. Information regarding variances and co-variances of error matrices are used to determine these confidence regions.

4.1.2 Apparatus and Analytical Technique

4.1.2.1 Composite Specimen

The effectiveness of any parameter estimation program depends largely on the associated experimental design. The physical model should be in close agreement with the theoretical model being utilized to extract the parameters. It is desirable to keep the physical model as simple as possible to avoid having to model phenomena that are not intrinsically related to elucidating the parameters of interest. Ideally the specimen would consist only of ER fluid and electrodes. The ER fluid however, needs to be contained in a gasket or holder. To be able to measure temperature profiles some means of attaching these thermocouples is necessary. There is an associated contact resistance with any attachment hence thermal pastes need to be utilized to minimize the contribution of this contact resistance to the effective thermal conductivity. Contact resistances are especially difficult to model. Also because of the electrical conduction in the electrodes, the thermocouples need to be electrically insulated. This requires the addition of another material. All of these materials need to be modeled in the mathematical description. With each additional layer some accuracy is sacrificed in the final estimates due to the challenge of finding adequate thermal property information on these materials. Contact resistances are also a concern between each interface. Accordingly, the composite materials and geometries were chosen so as to introduce the least possible amount of error.

Boundary conditions also need to be established. Since a constant temperature is difficult to apply and control, a resistance heating element was utilized to apply a constant heat flux to one side of the ER fluid. Because convection heat loss was expected from a

heater with one side exposed, a symmetrical configuration was utilized to ensure that the heat flux delivered to the fluid was accurately known. A constant voltage was applied to the heater, and it was assumed that the corresponding heat flux would be equally partitioned to both sides of the heater. Thermocouple measurements made at identical locations on either side of the heater were in very close agreement lending credence to this assumption. An air spacer was placed against the outer electrode of the composite specimen using a ring of Teflon gasket material. This was modeled as an insulated boundary condition because the thermal conductivity of air is very low and the duration of experiment was short. Heat loss from this boundary should be negligible in that time period. Figure 4.1 illustrates the materials that make up of one-half of the symmetrical composite specimen.



Figure 4.1 One-half of the symmetrical composite specimen: a) Teflon air spacer aluminum electrode c) Teflon gasket to contain the ER fluid d) aluminum electrode.

The most challenging aspect of the experimental design was thus selection of composite materials that were both appropriate for the experiment and had well-characterized thermal properties (a necessity for the parameter estimation algorithm). The choice of electrode material was flexible. The particular material chosen, McMaster-Carr

alloy 6061 aluminum, was done so on the basis of temper (T6) and thermal conductivity (167.27 W/mK). The material needed to be thin and highly thermally conductive to minimize error in the parameter estimation procedure. However to ensure that the thickness of the fluid layer was accurately known, it was essential that this material was very rigid. Buckling of the electrodes would cause a spatial distribution of electrode gap widths. These circular electrodes were 0.8128 mm thick with a 3.81 cm radius. Teflon gasket material of 3 mm thickness was used to contain the ER fluid between the electrodes.

Triple junction thermocouples were attached to the aluminum disk with a very thin layer of acrylic coating. This acrylic coating was so thin relative to the other materials it was not included in the model. Because of the voltage being applied to the aluminum disks, direct attachment of thermocouples was not possible. It was necessary to insulate the thermocouples from the high voltage environment to achieve high signal-to-noise ratios. Ideally a well-characterized, electrically insulating, thermally conducting material would be implemented. These are difficult properties to obtain in one material. Poly(vinyl)chloride tape provided an excellent electrical insulator but a poor thermal conductor. However its properties were known with some degree of accuracy. As such, it was used to insulate only the areas around the junctions. Although this introduces error into the Prop-1D estimation algorithm, it allows millivolt thermocouple measurements to be taken without a large degree of noise from the high voltage environment. Small sections of poly(vinyl)chloride (PVC) electrically resistant tape were placed on the electrode at the site of attachment of the thermocouple junctions. The thermocouples were

attached to the side of the electrode that was not in direct contact with the ER fluid. The triple junction thermocouple was attached to each aluminum disk as shown in Figure 4.2.



Figure 4.2 Triple junction T-type Copper-Constantan thermocouples attached to aluminum electrodes with poly(vinyl)chloride electrical tape backing.

These thermocouples were very sensitive to mechanical damage, however the space-averaging they provided reduced the amount of data-conditioning necessary before running the Prop-1D analysis. It is common practice to average and initialize the ambient thermocouple measurements. This feature is inherent in the design of the triple junction thermocouples.

To complete the construction of the composite specimen, two equivalent sets of ER fluid material, gaskets, and electrodes were then sandwiched together with a 0.28mm thick Kapton resistance heater at the center of the assembly. Before connecting these components a layer of high thermal conductivity Omegabond 200 thermal paste was affixed to each side of the heater to enhance the heat transfer and reduce the contact resistance between the heater and the electrodes. The fully assembled composite specimen is shown in Figure 4.3.



Figure 4.3 The fully assembled composite specimen.

The model of this composite specimen, as used for Prop-1D analysis is shown in Figure 4.4. Although only small sections of PVC tape were used to insulate the thermocouples, this tape was represented as a thin 3 inch diameter layer in the Prop-1D model.

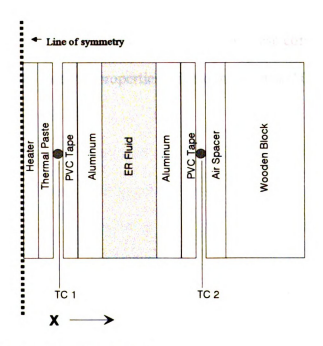


Figure 4.4 Model for Prop 1D Analysis.

In the interest of understanding the relative contributions of the thermal conductivities of the individual materials to the overall effective thermal conductivity of the specimen, it is worthwhile to examine the steady-state response of the composite specimen to constant temperatures imposed on either side. This abstraction permits the consideration of these materials as thermal resistances in series via:

$$q = \frac{T_1 - T_n}{(\Delta X_{kA})_1 + ... (\Delta X_{kA})_n} = \frac{\text{Total Thermal Potential Difference}}{\text{Sum of Thermal Resistances}}$$
[4.1]

Although having no numerical significance in the transient measurements, knowledge of $\Delta X/k$ would give an indication as to its sphere of influence in the total thermal resistance. Thus a calculation of $\Delta X/k$ for each of these materials is very constructive for evaluating the effects each material has on the overall thermal conductivity, and on the optimization of the experiment in general. The results of these computations are shown in Table 4.1, along with the material properties utilized in the Prop-1D algorithm.

	Thickness (m)	Volumetric Specific Heat (10 ⁻³ kJ/m ³ K)	Thermal Conductivity (W/mK)	ΔX /k
Kapton Heater ¹	0.00014	1.871	0.980	1.429x10 ⁻⁴
Omegatherm 200 Paste	0.00034	1.369	2.307	1.474x10 ⁻⁴
PVC Tape ²	0.00016	1.334	0.168	9.524x10 ⁻⁴
Aluminum	0.0008128	2.463	167.27	4.859x10 ⁻⁶
ER Fluid ³	0.003	3.566	0.105	2.86 x10 ⁻²

Table 4.1 Material properties of components used in the composite specimen.

It can be seen that $k_{c\text{-eff}}$, the effective thermal conductivity of the composite, depends mostly on the $k_{f\text{-eff}}$, the effective thermal conductivity of the ER suspension. This would imply that any inaccuracies in the thermal property information of the peripheral materials (electrodes, PVC tape, etc.) should not have a dramatic effect on the accuracy of the estimation of the thermal properties for the fluid. Although the model is complicated by the presence of additional materials, the effects on the accuracy of the output should be minimal.

4.1.2.2 Data Acquisition System

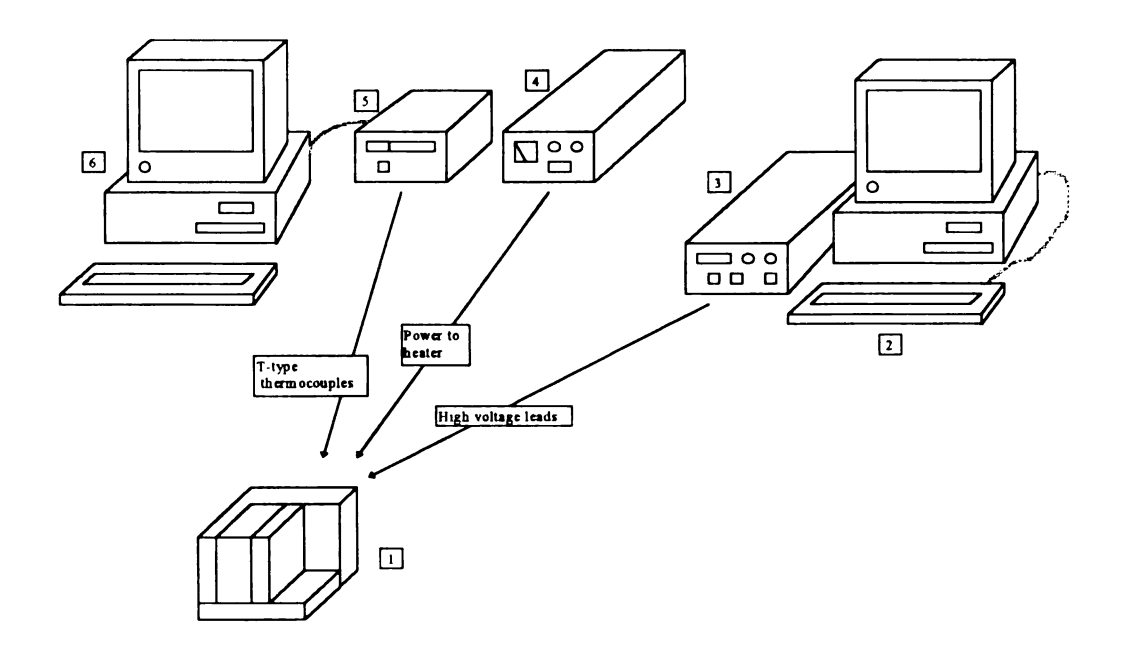
The data acquisition system used for thermal property estimation is detailed in Figure 4.5. Because of issues regarding shielding of thermocouple measurements as well as amplification of signals, the Fluke Hydra 2065 data logger was implemented for obtaining temperature profiles. The data logger holds information in its internal memory which is then uploaded through an RS-232 interface to a 486 computer at the end of each

¹ Values obtained from measurements made by Beck, 1996

² Properties for PVC, Handbook of Plastics

³ Previously published work (Lloyd, 1994)

experiment. The signal-to-noise ratio of temperature measurements using the data logger was excellent however the scan time per channel was on the order of 1 second, lengthy in terms of ideal design of experiment criteria. This did not allow for acquisition of multiple sensor measurements in a reasonable time period. To circumvent this limitation, bare wire butt-welded Copper-Constantan triple-junction thermocouples were implemented, the construction of which is outlined in Appendix B.



Components:

- 1) Composite specimen
- 2) 7100/80 PowerMacintosh with Labview software, used as a voltage controller
- 3) Trek 2025 high voltage DC power supply and amplifier
- 3) Hewlett Packard DC power supply
- 4) Hydra Fluke data logger equipped with T-type thermocouple sensors
- 5) 486 computer / RS-232 interface

Figure 4.5 Data Acquisition System

4.1.3 Governing Equations and Boundary Conditions:

The ratio of diameter to thickness of the plates used in the heat conduction apparatus was quite large (\sim 75:1), hence heat conduction in the transverse direction was assumed to be negligible. Convective effects in the fluid were neglected because of the small scale involved and the associated small Raleigh number. It was also assumed that thermal conductivity did not vary in the x-direction. In actuality the thermal conductivities in both the chained and the randomly dispersed states are anisotropic due to the inhomogeneous nature of the suspension. The anisotropy is more pronounced when the particles are chained. For the purposes of these experiments however, the medium was assumed to be homogeneous. The value of k estimated for ER suspensions is thus an effective thermal conductivity, k_{f-eff} , representing the combination of both the particles and the carrier medium.

The resulting heat transfer problem is thus represented by a 1-dimensional transient heat conduction mathematical model:

$$\frac{\partial^2 \mathbf{T}}{\partial \mathbf{x}^2} = \frac{1}{\alpha} \frac{\partial \mathbf{T}}{\partial \mathbf{t}}$$
 [4.2]

where, T is temperature (K), x is distance (m), t is time(s), and α the thermal diffusivity (m²/s).

The boundary conditions are given by:

$$-k_{eff} \frac{\partial T}{\partial x}\Big|_{x=0} = q_0$$
 constant heat flux at x=0 [4.3]

$$\left. \frac{\partial \mathbf{T}}{\partial \mathbf{x}} \right|_{\mathbf{x}=L} = 0$$
 insulated at $\mathbf{x}=\mathbf{L}$ [4.4]

and the initial condition by:

$$T(\mathbf{x},0) = T_{\mathbf{i}} \tag{4.5}$$

The analytical solution, using Green's functions (Carlslaw and Jaeger, 1959), is:

$$T(x,t) = \frac{q_0 L}{k_{eff}} \left[\frac{\alpha t}{L^2} + \frac{2}{\pi^2} \sum_{m=1}^{\infty} \frac{1}{m^2} \cos \left(m \pi \frac{x}{L} \right) \left(1 - e^{-m^2 \pi^2 \alpha t / L^2} \right) \right] [4.6]$$

In dimensionless form this solution is written as:

$$T^{+}(x^{+},t^{+}) = t^{+} + \frac{1}{3} - x^{+} + \frac{1}{2}(x^{+})^{2} - \frac{2}{\pi^{2}} \sum_{n=1}^{\infty} \frac{1}{n^{2}} e^{-n^{2}\pi^{2}t^{+}} \cos(n\pi x^{+})$$
 [4.7]

where,

$$T^{+} = \frac{T - T_0}{qL / k_{\text{eff}}}$$
 [4.8]

$$t^{+} = \frac{\alpha}{L^{2}}t$$
 [4.9]

and,

$$\mathbf{x}^+ = \frac{\mathbf{x}}{\mathbf{L}} \tag{4.10}$$

4.1.4 Data Analysis

Once the appropriate mathematical model and physical experiment were established, temperature profiles were obtained to extract the desired parameters. Data acquisition was initiated and a constant voltage applied to the Kapton heater to deliver a known and constant heat flux to the composite specimen. The Kapton heater was powered by an Hewlett Packard 6024A D.C. power supply. Before experimentation the resistance of the heater was measured with a Textronix hand-held digital multi-meter, as was the exact voltage supplied to the heater. It was assumed this output remained constant over

the duration of the experiment. The heat flux was applied for a pre-determined period of time. Data acquisition was continued for a period of time after turning off the applied heat flux.

When the test was complete the data logger memory was uploaded through the RS-232 interface to the hard drive of the 486 computer. A temp.dat file was created by the Starter software which stored the uploaded information. A short Quick-Basic program was utilized to translate the data logger time stamp to seconds and to put the temp.dat file into a text format which could be edited for input to Prop1D. This program is listed in Appendix C.

Prop-1D required two input files. The first file, the input control parameter file (*.icp), contained the experimental design parameters such as composition of the specimen, corresponding thermal properties and dimensions, duration of experiment and sensor location. Initial estimates of the thermal properties of interest are also included in this file. The second file (*.txt) contained the discrete temperature measurements at each location, as well as the applied heat flux history. The generated output file (*.out) included a record of the input control parameters, the temperature data, estimates of the desired parameters and also information about 95% confidence intervals, sequential estimates, residuals, and sensitivity coefficients, all of which gave valuable information about the validity of results as well as insight into how the experiment should be redesigned. A sample of each of these files is contained in Appendix D.

4.1.5 Experimental Method

It was expected that the thermal properties of the ER fluids in the isotropic state would be very similar to that of the carrier fluid alone. Silicon oil was thus utilized for the design of experiment, as its properties were already well-established, and could better guide the optimization process. The details of the experimental design are contained in Appendix E. When this experiment was satisfactorily optimized, water was evaluated to test the experiment's reliability and accuracy for evaluating other fluids. Finally, the ER suspensions were examined in zero DC field and low DC field conditions.

4.1.6 Results and Discussion

Shown in Figures 4.6 and 4.7 are the results of a series of analyses on silicon oil. The duration of experiment was 84 seconds, with an applied heat flux of 1907 W/m² for 48 seconds. This duration of heating and data collection was calculated from the Fourier number, which is detailed in Appendix E. It can be seen from Figure 4.6 that the values obtained for thermal conductivity were reproducible to within 4%. When the average of replicate measurements was compared to the literature value for silicon oil at 50°C the agreement was within 8%. Conversely for volumetric specific heat measurements, as shown in Figure 4.7, the deviation from the mean was as much as 8 %. The reference value for volumetric specific heat measurements was obtained by multiplying the listed manufacturer's value for density at 25°C by the value for specific heat as measured by DSC at 25°C. The C_p value at this temperature was not provided by the manufacturer however the DSC measurements at the higher temperature were in agreement with the

manufacturer's listed higher temperature values, lending credence to the DSC analysis. When this reference value for volumetric specific heat was compared to the average of replicate measurements, the agreement was within 13%.

Estimates of Thermal Conductivity (k) of Silicon Oil Applied Field Strength: 0 V/mm

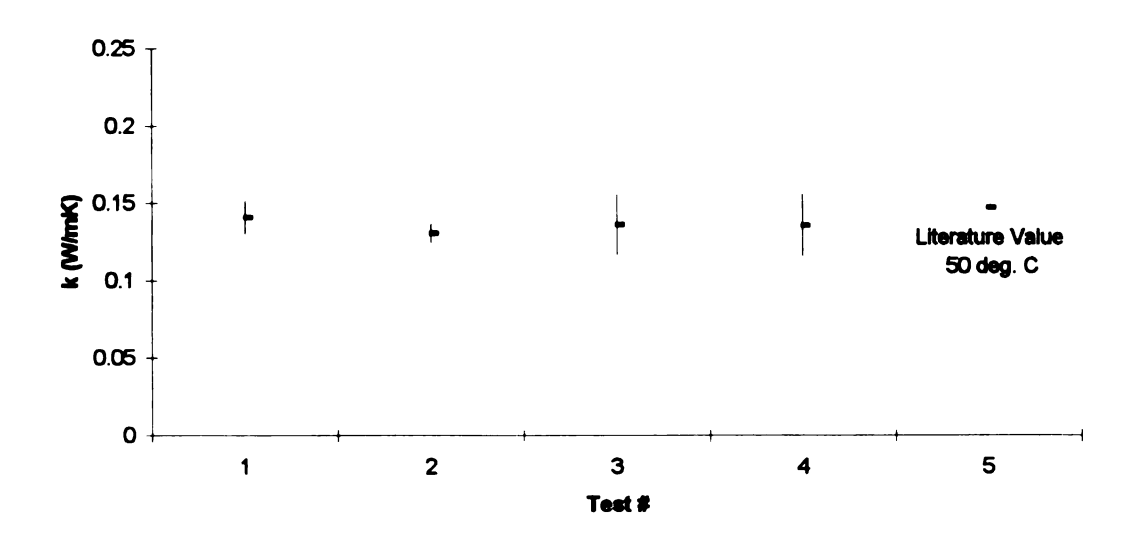


Figure 4.6 Estimates of thermal conductivity of silicon oil.

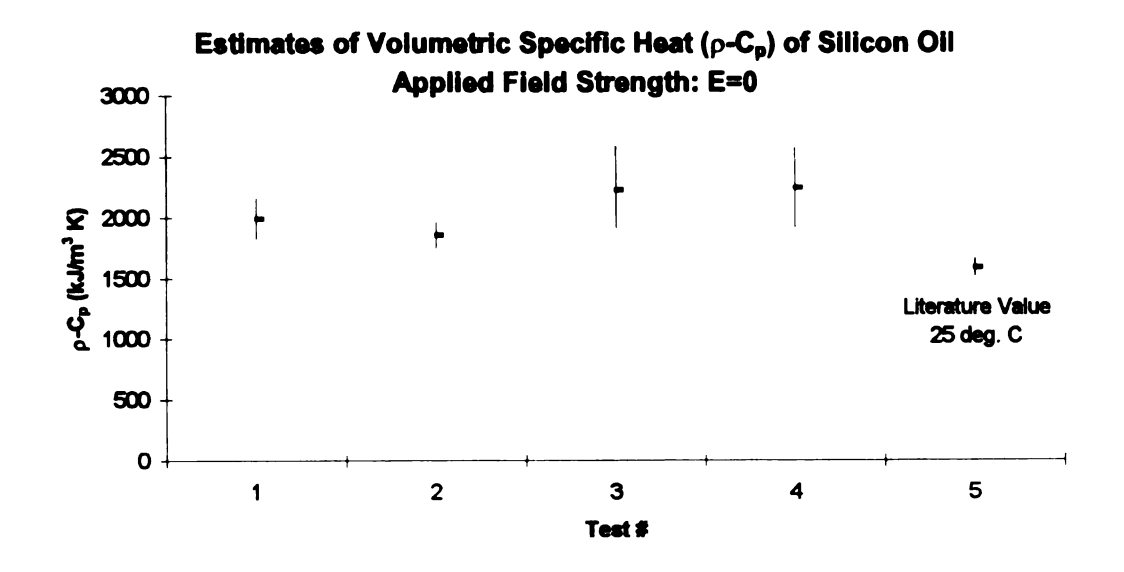


Figure 4.7 Estimates of volumetric specific heat of silicon oil.

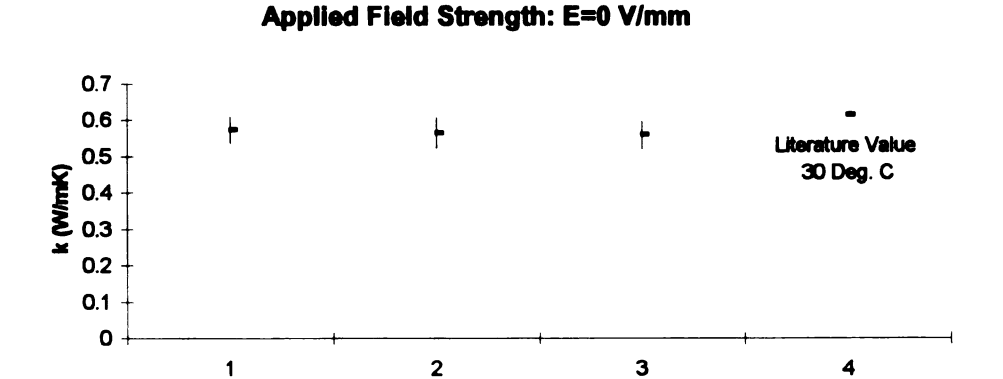
It is hard to compare these numbers precisely because the measured values represent an average of the parameters over the temperature range that evolves due to application of the constant heat flux. Literature values for thermal conductivity were available only at a single temperature. In the transient experiments, the dynamic temperature range was 23 to 40 °C. For the purposes of the optimization it was assumed that over the 20 to 50 °C temperature range, the thermal conductivity and the volumetric specific heat remained relatively constant.

The inability to obtain multiple data points in a relatively short period of time prevented the measurement of the contact resistance in the system and thus complicated the results. It was expected that this would be included in the estimate for the thermal properties of the ER suspension. This is consistent with the slightly lower estimated values of thermal conductivity. This however does not explain why the volumetric specific heat estimates are consistently higher than the reference value. An examination of the residuals indicated some correlation in errors, two-dimensional heat losses, as well as some irregularity in the sequential estimates for volumetric specific heat, as is discussed in Appendix E. The sequential estimates did not approach a constant value and stabilize, but instead were somewhat erratic in nature. This indicated that the model was not in perfect agreement with the physical experiment and that there was a possible identifiability problem with determining both parameters simultaneously.

Despite the problems identified with the experiment, the reproducibility and relative accuracy of the measured parameters were considered adequate from the standpoint of evaluating thermal property changes due to electrorheological response, as property changes of several hundred percent were expected. To ensure that the

experiment could perform equally well for other types of fluids and with the same level of accuracy, water was also evaluated.

For the water analyses the duration of the experiment was 54 seconds, with an applied heat flux of 1906 W/m² for 30 seconds. The results of these analyses are given in Figures 4.8 and 4.9. It can be seen that the estimates of thermal conductivity for water are similar to those of silicon oil. When compared to the literature value at 30 °C, the agreement is within 8%. Again the estimates are consistently lower than the reference value, concordant with the unmodeled contact resistance. Replicate measurements agreed to within 2%. For the volumetric specific heat measurements agreement among replicate analyses was within 3%, however comparison of the experimental mean and the literature value gave agreement to within 25%. Similar irregularities were observed in the sequential estimates, and the residuals had the same character as those obtained for the silicon oil experiments.



Test#

Estimates of the Thermal Conductivity (k) of Water

Figure 4.8 Estimates of thermal conductivity of water.

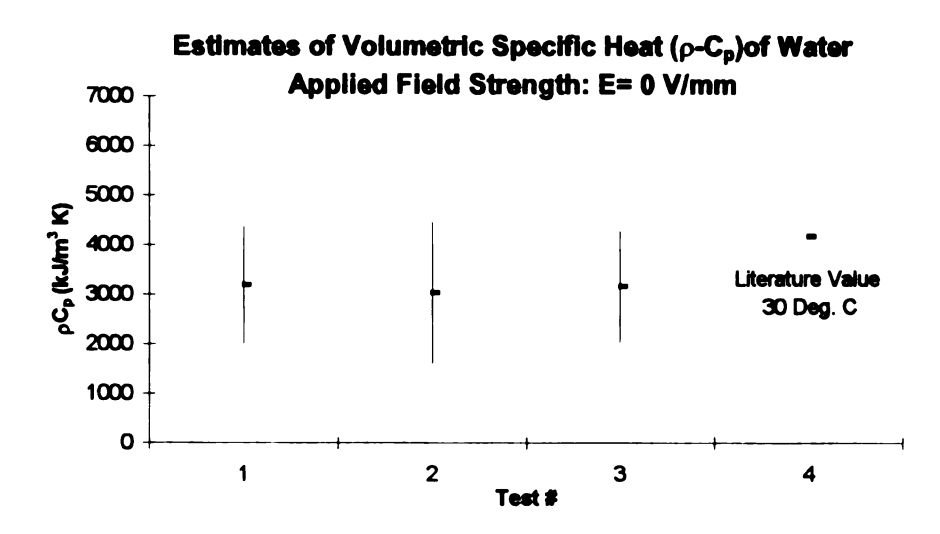


Figure 4.9 Estimates of volumetric specific heat of water.

Based on the results of these experiments with silicon oil and water it can be reasonably concluded that using this experimental method it is possible to reproducibly generate a number that should be a sufficiently accurate measure of the thermal conductivity of isotropic suspensions to evaluate property changes. Volumetric specific heat measurements were not as reliable in terms of an accurate representation, and the sequential estimates raised suspicions as to the significance of the measurement. The parameters however were reproducible and thus can be cautiously used to evaluate property changes. Given the limits of reproducibility, thermophysical property changes less than 5% could not be considered statistically significant.

Isotropic ER Fluid suspensions were evaluated without application of electric fields. The experimental duration was 108 seconds with an applied heat flux of 1906.2 W/m² for 108 seconds. Again reproducibility was within 3%. Sequential estimates and residual analyses were consistent in character to the previously obtained results for silicon oil and water, indicating that the non-idealities of the experiment were systematic in nature.

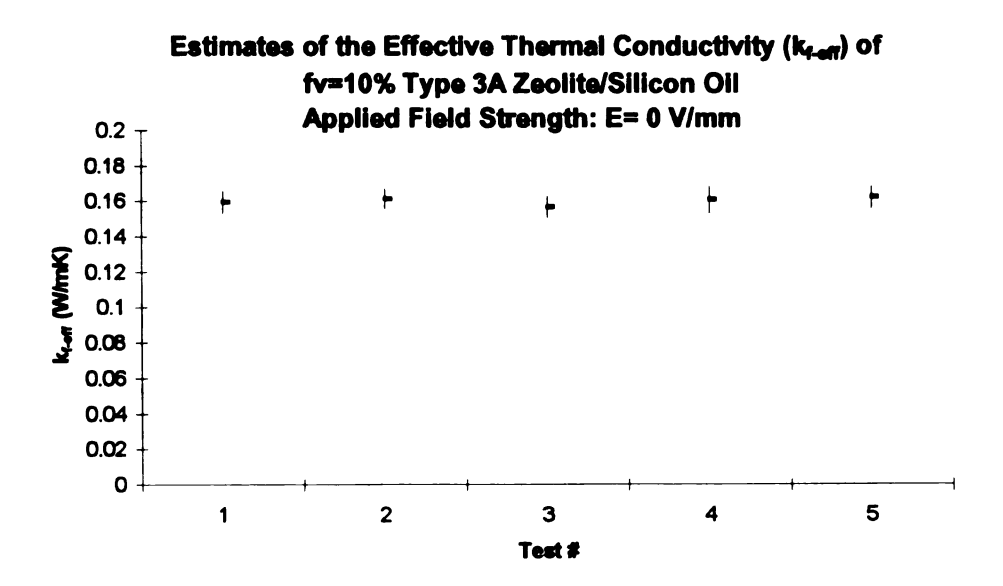


Figure 4.10 Estimates of the thermal conductivity of 10% volume fraction Type 3A zeolite/ silicon oil.

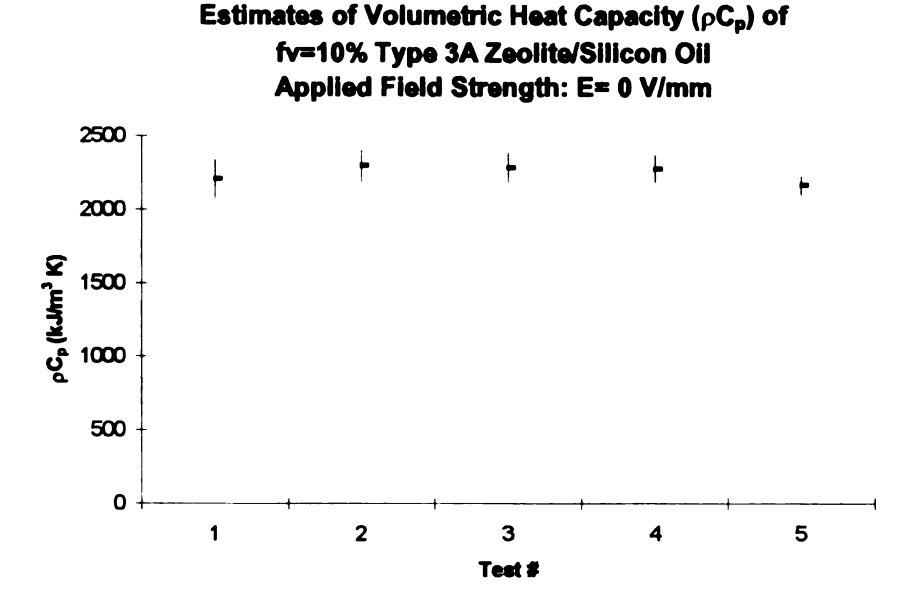


Figure 4.11 Estimates of the volumetric specific heat of 10% volume fraction type 3A zeolite/silicon oil

The value of thermal conductivity measured for the 10% volume fraction ER suspension was higher than that of silicon oil alone. This was an unexpected result. Also a general observation was a fluctuation in the estimated properties for the same volume fraction fluids prepared on different days. This fluctuation was highly likely due to moisture content variations. To further explore these observations measurements, a series of ER suspensions of different volume fractions were prepared on the same day and evaluated. The results of these analyses are shown in Figure 4.12. The wet and dry suspensions were made according to the method presented in Chapter 2.

Thermal Conductivity (W/mK) vs. Volume Fraction (f_v) Applied Field Strength: E=0 V/mm

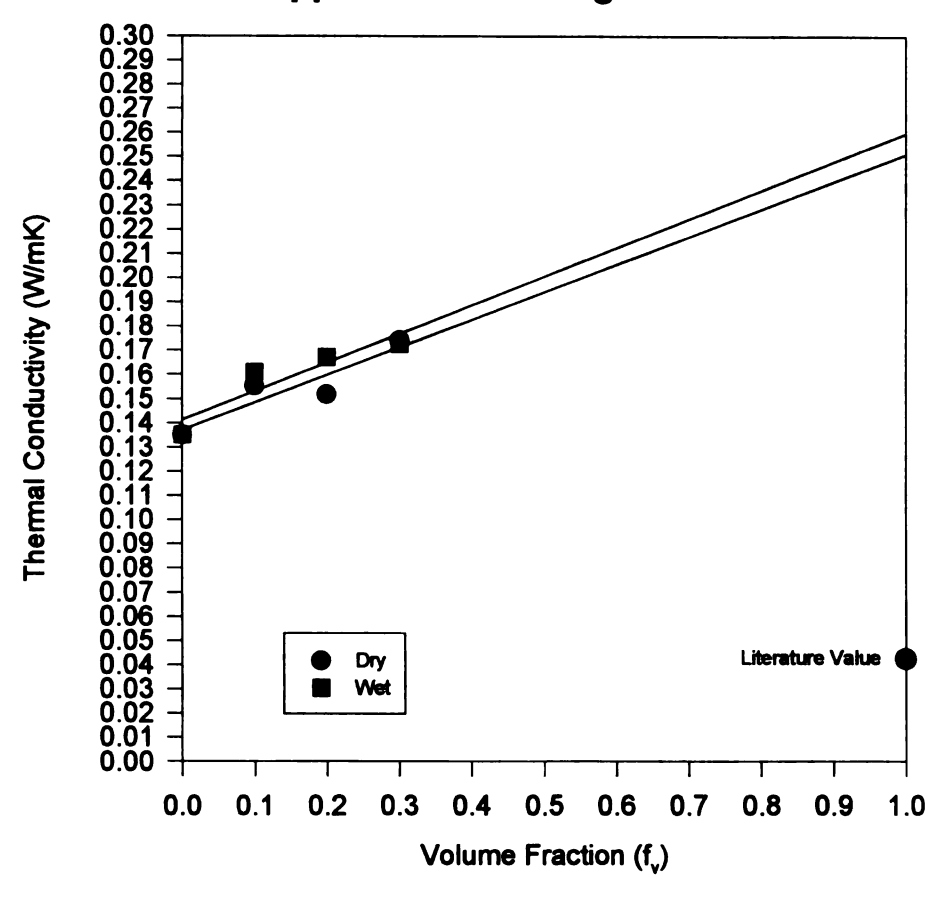


Figure 4.12 Estimates of thermal conductivity of a wet and dry series of type 3A zeolite/silicon oil suspensions.

It can be seen that the thermal conductivity increases with increasing volume fraction of zeolite particles which seems counter-intuitive based on the values of thermal conductivity for zeolite and silicon oil (0.04 and 0.1407 W/mK, respectively). As discussed in Appendix A, zeolites are aluminosilicate cage arrays. A measurement of the thermal conductivity of this material will necessary include the presence of large pockets

of air in the cavities of the sodalite cages. In its dry-packed state the zeolite will behave as porous media, serving to reduce the heat transfer by restricting the movement of air in the cavities (Zeng et. al., 1995). It is informative to compare the thermal conductivities of air with the aluminum oxide and silicon dioxide that comprise the framework of zeolite crystals (Table 4.2). It is likely that when the zeolite is suspended in the silicon oil, the air pockets are no longer present and the contribution of the zeolite to the effective thermal conductivity is dominated by the zeolite's structural elements. These values are seen to be substantially higher than those of silicon oil hence small amounts of zeolite can have significant effects on the thermal conductivity.

	k (W/mK)
aluminum oxide, sapphire	46
aluminum oxide, polycrystalline	36.0
Silicon dioxide, crystalline	6.21-10.4
silicon dioxide, polycrystalline	1.38
air	0.026

Table 4.2 Thermal conductivity values for aluminum oxide and silicon dioxide (Gebhart, 1993).

It can be concluded that in the range of volume fractions typical of ER fluid applications, the zeolite serves to increase the thermal conductivity, not decrease it. In general, the effective thermal conductivity does not decrease linearly from the value of thermal conductivity for pure silicon oil, 0.14 W/mK, to the value for pure zeolite, 0.04 W/mK. The relationship between volume fraction zeolite and effective thermal conductivity is thus non-linear.

It has been established that reproducible values are possible to obtain for water, silicon oil and the isotropic ER suspensions via the adapted 1-D transient heat conduction apparatus. Measurements in high voltage fields were attempted next. These measurements proved to be considerably more challenging.

Shown in Figures 4.13 and 4.14 are the results of applying low field strengths to a 5% volume fraction of an ER fluid suspension. The microscopic evaluation of the 2% suspensions indicated that low field strengths may be adequate to ensure substantial chaining, despite the fact that almost all applications discussed in the literature utilized electric fields of several thousand volts. As can be seen from the estimated results however, no change in thermal conductivity or volumetric specific heat were observed at these field strengths. It is possible that chaining did indeed occur, but the effective thermal conductivity, although different in character, was the same in measured magnitude.

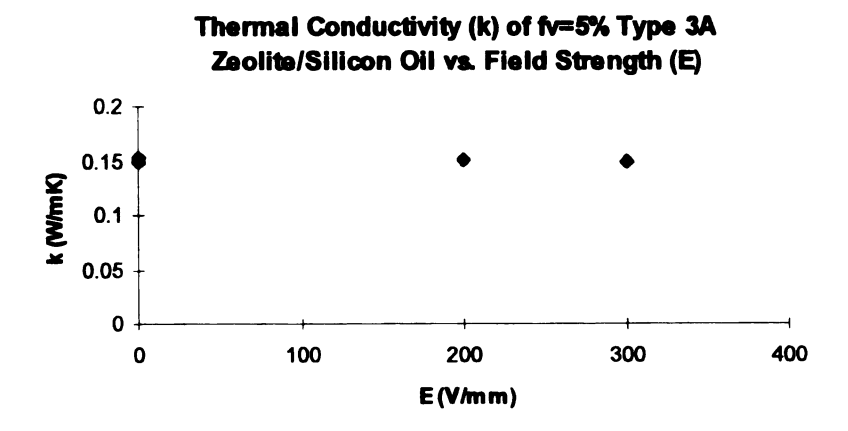


Figure 4.13 Thermal conductivity of $f_v = 5\%$ Type 3A zeolite/silicon oil suspension at low field strengths.

Volumetric Specific Heat (ρC_p) of fv=5% Type 3A Zeolite/Silicon Oil vs. Field Strength (E)

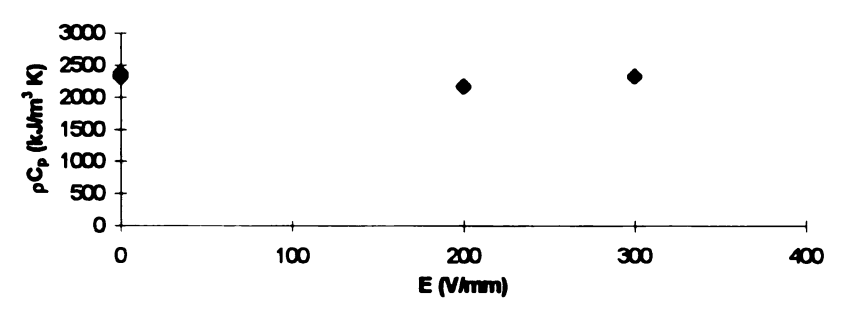


Figure 4.14 Volumetric specific heat of $f_v = 5\%$ Type 3A zeolite/silicon oil suspension at low field strengths.

Similarly for higher volume fractions, no significant change in properties was evident. Shown in Figures 4.15 and 4.16 are the thermal conductivity and volumetric specific heat estimates for $f_v = 10\%$ and 20% suspensions.

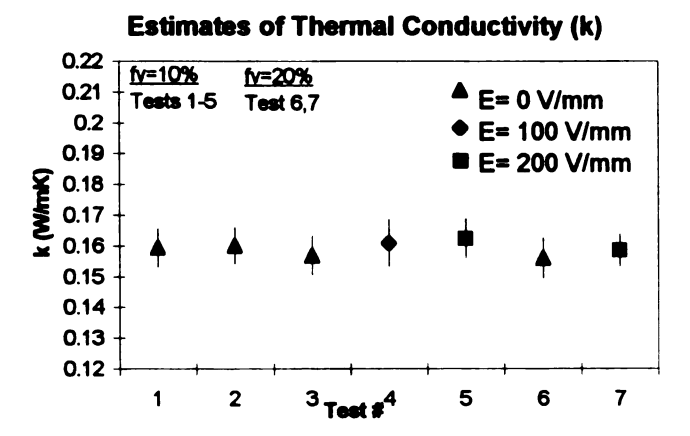


Figure 4.15 Thermal conductivity of $f_v = 10\%$ and 20% Type 3A zeolite/silicon oil suspension at low field strengths.

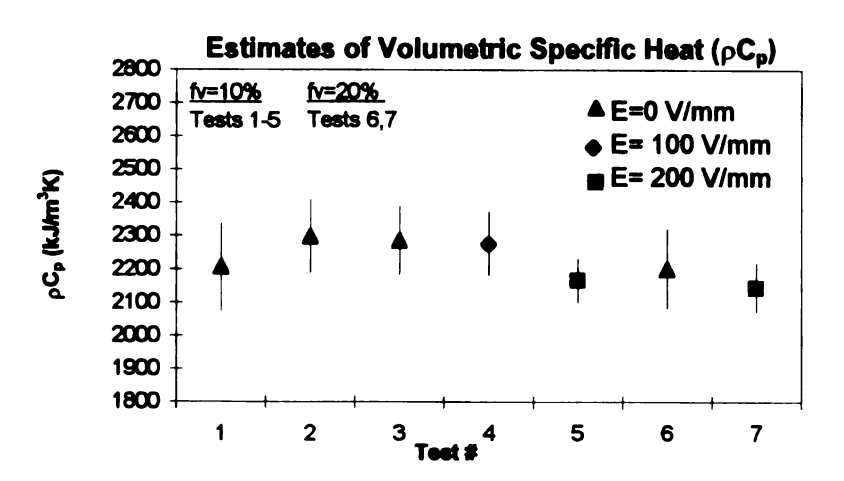


Figure 4.16 Volumetric specific heat of $f_v = 10\%$ and 20% Type 3A zeolite/silicon oil suspension at low field strengths.

Upon application of higher field strengths, several difficulties were encountered. When electric fields were applied in excess of a certain field strength characteristic of each individually prepared fluid, the electrical conductivity quickly increased to a point where the high voltage amplifier current limited at 5 mA. This caused the voltage to drop to maintain Ohm's law, thus not allowing the voltages typically associated with intense chaining activity to be applied. Significant heat generations were observed when the current climbed to these limiting levels, sometimes as much as 10°C in a few seconds, depending on the electric field demanded and on the particular fluid. In some cases, at low field strengths, applying a heat flux to the system caused the current to increase to a point where the amplifier rapidly current limited, thus further limiting the upper range of field strength. At lower current levels the heating was less extensive but was indeed present. Coupled with this limiting situation was the appearance of bubbles in the system

and evidence of deterioration of the electrode surfaces upon disassembly of the apparatus.

The ER fluid was also observed to flow out of the apparatus indicating significant levels of expansion.

Shown in Figure 4.17 is an example of a temperature rise in the fluid due to application of a 500 V/mm field. In this example the temperature rises were very small over short time periods, or the typical duration of a parameter estimation experiment. As was oftentimes the case however, this temperature rise was not negligible in comparison to the temperature rise due to application of the heat flux necessary to measure the The electrical response of the manufactured ER fluids was very unpredictable, and seemed to be heavily dependent on the ambient humidity conditions The field-dependent temperature response was during manufacture of the fluids. observed to qualitatively correlate with the electrical conductivity of the fluids, and consequently with the water loading in the ER fluid. Fluid manufacture and experimentation were not carried out under controlled humidity conditions and oftentimes exposure to excessive levels of high temperature steam was unavoidable. The result was greatly fluctuating responses to electric field conditions making quantification of phenomena difficult.

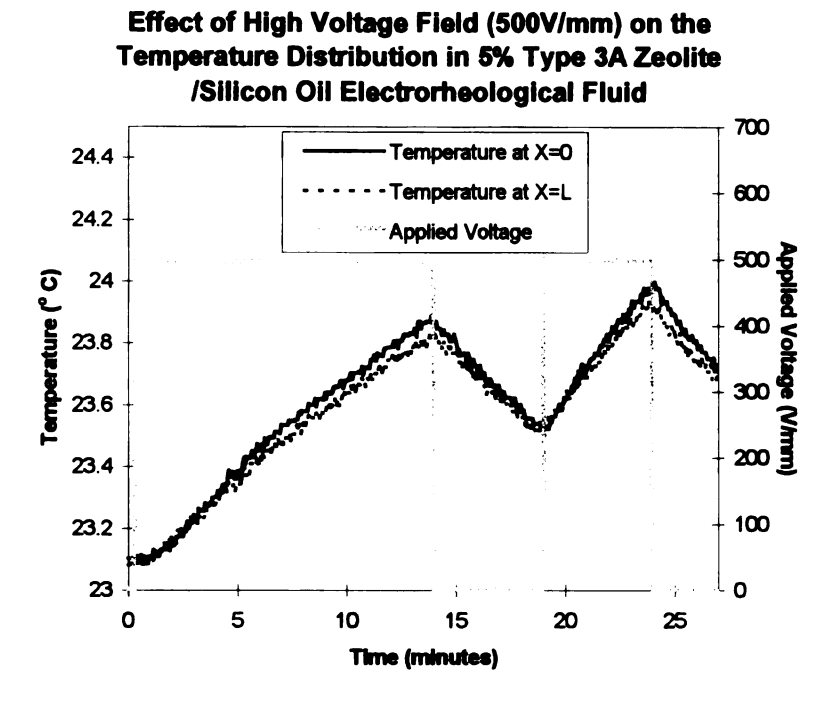


Figure 4.17 Effect of electric field on the temperature distribution in the ER fluid system.

This resistance heating is not a new phenomenon. Lee et al. (1993) and Nelson and Suydam (1993) have indicated that power consumption in ER fluids increases with increasing field strength and with increasing temperature, consistent with general electrical theory. Before judicious modifications can be made to circumvent this problem, a means of quantitatively characterizing this temperature response as a function of current is necessary. This requires an analysis of the underlying mechanisms responsible, as well as a modeling of the response in the form of a predictive model.

Zhang and Lloyd (1993) indicated 50% change in the value of k with the application of a 760 V/mm AC field. There are several reasons why this may not be easily achievable with DC fields. It is becoming well-established (Foulc et al., 1996; Davis, 1992a; See et al., 1996) that in high frequency AC fields, the governing parameter

in ER activity is the complex permitativity mismatch, whereas the values of electrical conductivity of the individual components of the ER fluid represent the dominant controller in low frequency AC or DC conditions. Thus a material which is ER active when utilized with AC fields, may not be effective in DC field conditions.

Foulc et. al. (1996) have suggested a ratio of solid to liquid electrical conductivities in excess of 100 to ensure significant ER effects. More specifically Boissy et al. (1996b) have indicated that a practical conductivity guideline of 10^3 $\sigma_L < \sigma_S < 10^{-7}$, where σ_L and σ_S are the electrical conductivities of the liquid and solid phases, respectively, for DC fields. As seen from Table 2.1, the conductivity mismatch from zeolites and silicon oil may or may not satisfy these criteria. As previously indicated, somewhat crude humidity control was attempted with the zeolites to control the conductivity of the solid phase. It was found that more sophisticated equipment was necessary to achieve reproducible water-loadings. Humidity control in the liquid phase was not given priority consideration because of its weak hydrophilicity in comparison to Results by Wu et al. (1996) have indicated that this may be a poor the zeolite phase. assumption. Wu et al. found that the current density and electrical conductivity of Dow Corning 200 silicone oil increased with electric field strength and water content. Control of water content and evaluation of electrical properties of both phases are thus emerging as essential ingredients to designing a successful ER fluid.

Qiu et. al. (1996) in a comparison of the temperature dependence of AC and DC conductivities, found evidence that charge carriers respond differently to AC and DC fields. It was found that the dielectric loss could be divided into two parts, one part originating from DC conduction and the other portion from the AC response of bound

charges inside the particle. When the difference between these is small, there is little evidence of ER activity, whereas the converse is true when these components of dielectric loss differ greatly. It was found that in an atomite ER fluid this difference was small below 250 K but was greatly increased above 300 K. In the experiments by Zhang & Lloyd the applied heat flux resulted in a final temperature of 320 K. If the zeolite suspension behaves similarly, this higher temperature might have favorably enhanced this dielectric loss component difference.

The estimation routine for the sample investigated in Zhang and Lloyd (1993) was such that the experimental duration was 600 seconds. This is not precisely in accordance with the optimal heating time for this experimental design and, as shown by the sequential estimates in Appendix E, an estimate based on measurements attained over varied experimental durations can yield dramatically different results. This may have affected the final values and may have introduced error into the final results.

It is possible that property changes could be observed for these fluids under DC conditions if higher field strengths could be utilized. In the interest of improving the range of field strengths over which the property estimation could be carried out, an attempt was made to quantify the temperature rises in the ER fluids due to application of electric fields, in an order-of-magnitude sense. The relationship between the suspected Joule heating and the resulting temperature rise can be given by:

$$V\rho C_{p} \frac{\partial \Gamma}{\partial t} = I^{2}R$$
 [4.11]

and thus the temperature rise is by:

$$\Delta T = \frac{EI}{V\rho C_p} \Delta t$$
 [4.12]

where E is the applied field (V), I is the current (A), R is resistance (Ω), V is volume (cc), ρ is density (g/cc), and Δt is the time period of interest. The Cp data utilized in this calculation was obtained from MDSC analysis of the zeolite suspension. These measurements are outlined in Appendix F. Using the nominal values given by: E=485V, I=5mA, V=7cc, ρ =1.25 g/cc, C_p =1.3 J/g°C and Δt =60s, the expected temperature rise was determined to be on the order of 13°C. The experimentally observed value under these conditions was approximately 2°C. This would seem to indicate that there were also other interferences in the system besides pure Joule heating. Stangroom (1996) has pointed out that the currents generated in ER fluids are non-Ohmic. He utilized a quadratic model of current with constants characteristic of the fluid. Despite the fact that these order-of-magnitude calculations are based on an Ohmic assumption, the results indicate in a qualitative sense, that thermal energy dissipations are to be expected in these high current systems.

If the temperature rises due to application of the field are comparable to those due to the imposed heat flux, the 1-D transient heat conduction model will no longer be appropriate. A new mathematical model including a source term for Joule heating and possibly other phenomena would be necessary to represent what is physically occurring in the ER system. This would become a very complicated problem to solve, and would preclude the use of PROP-1D for parameter estimation.

As pointed out in Chapter 2, microscopic particulate matter was observed to dissociate from the electrode during the application of high voltage fields. Boissy et. al. (1996a) have considered the effect of electro-chemical processes occurring at the electrode interface on current density. It was suggested that a second component of current density results from injection of electrode ions into the solution when high voltage fields are applied, which could potentially control the current levels generated. This seems consistent with the previous observations of excessive current levels, and evidence of a chemical reaction at the electrode surface. If the particulate matter which is originating at the surface is a charged metal ion then it is likely to be highly conductive. This has other ramifications.

See et. al. (1996) have investigated the effect of adding small amounts of highly conductive particles to ER fluids. A marked decrease in the viscosity change characteristic of the fluid was observed. If charged metal particles are entering into the ER suspension it is likely that they will affect the structure formation. This serves to further complicate the observed results.

In terms of the ER fluid flowing from the gasket material in high current situations, it appears as if the fluid is boiling, however the temperatures are nowhere near the levels necessary for this to occur. Consistent with microscopic imaging observations, hydrolysis of water and the associated evolution of hydrogen gas seems to be a likely source of the bubbles. The expected expansion of the fluid under these temperature conditions can be calculated from:

$$\beta = \frac{1}{V} \frac{\partial V}{\partial \Gamma}$$
 [4.13]

where β is the coefficient of expansion. For silicon oil this value is 0.00043. This yields an expected volume change of 0.045 cc for a 15 degree temperature change, which corresponds to a 0.6 % expansion. This would not cause the material to flow from the gasket hence the temperature rise due to heating is not the source of this phenomenon.

At low field strengths, the electrical behavior was indicative of chaining activity (McGregor, 1997), however no measurable change in thermal conductivity was measured. Field strengths typical of ER fluid applications are upwards of several thousand volts. These voltages would be catastrophic to the system under study. Within the limits imposed by electrical conduction in the system, a change in effective thermal conductivity was not discernible at the field strengths possible.

McGregor(1997) has worked on a control algorithm which effectively controls the electrical conductivity of a given fluid by altering the voltage applied, however the control is limited to the ability to manipulate the moisture content, as the fluid will operate only in a range predetermined by the inherent conductivity of the particles. The moisture content of the zeolite affects the surface charge density on the particles, increasing the dielectric constant, and affecting the formation of the electric double layer. Conrad et al. (1994) examined the effect of heating on the electrical an mechanical properties of zeolite/silicone oil suspensions. The conductivity of the suspensions increased with particle concentration and water content heating, decreased the permittivity. The electrical conductivity of the suspensions is directly related to this double layer development and the underlying surface conditions.

To continue working with the zeolite/silicon oil systems it will first be necessary to determine the levels of water-loading that yield appropriate values of effective electrical conductivity. The mismatch between the conductivities of the suspending phase and the dispersed phase are important to maximize the ER response in DC field conditions. However, to ensure the minimization of heating due to current dissipations the effective electrical conductivity needs to be maintained below certain levels. If this can be achieved, the current 1-D transient heat conduction procedure can be utilized to measure the thermal properties of chained ER suspensions at higher field strengths.

4.1.7 Error Analysis

There are a variety of aspects of this experiment which could be isolated as contributing some degree of error to the experiment. Because of the time required by the data logger to scan each channel, the time interval necessitated to ensure equal time increments was 3 s. This is a substantial interval given that the duration of the experiment is on the order of 1.5 minutes. Reduced intervals would be desirable however with the current apparatus, the limit has been reached. Alternate temperature acquisition equipment could provide reduced time intervals, however the cost to ensure quality signals would be substantial. A data acquisition board and amplification system would be necessary.

The timing of the heat flux application was done manually with a stop watch. A controller online with experiment to start the heater and indicate the precise time of application would assist in the parameter estimation routine.

An evaluation of the residuals revealed significant correlations indicating the presence of systematic errors. Further optimization of the experiment in terms of the contact resistance could possibly reduce some of these errors. Also, the use of triple junction thermocouples instead of multiple sensors is likely to have some adverse effect on the correlation of errors. Alternate temperature acquisition equipment would probably improve the situation. One of the preliminary assumptions was that systematic effects were removed from the system such that the remaining errors were considered to be random. This was not the case. The residuals also provided information about the boundary conditions. The residuals drifted down near the end of the experiment, indicative of heat losses at the x=L boundary.

An error and sensitivity analysis incorporating these estimated measurement errors can be found in Appendix G.

4.2 Steady-State Measurements

Because of the complex nature of the electrical behavior in the ER system and the associated temperature response of the generated current, it was difficult to model the current behavior in the transient heat conduction model. A simpler steady-state method was evaluated for its potential for determining the thermal conductivity in high field situations.

The apparatus used for the steady-state experiments was essentially the same as for the transient measurements except the air spacer was removed and free convection was allowed to occur at the x=L boundary. As in the transient measurements a heat flux was quantified and applied. Instead of measuring temperature profiles, the temperature

difference across the specimen was measured once the specimen reached steady state. The applied heat flux had to be considerably higher to ensure that this temperature difference was resolvable. It took approximately 2 hours for the specimen to come to steady-state conditions when the applied heat flux was 471.6 W/m². A sample steady-state temperature profile is shown in Figure 4.18.

Steady State Temperature Profiles f_v=15% Zeolite/Silicon Oll

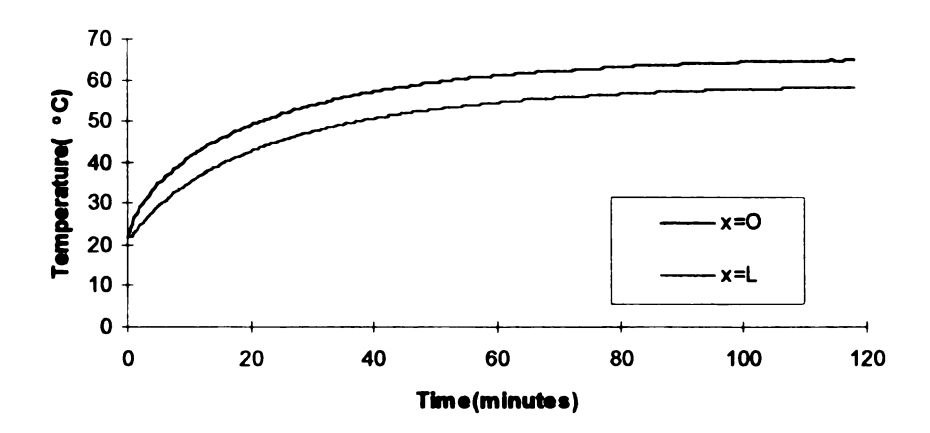


Figure 4.18 The temperature profiles measured across the composite specimen as the steady-state condition developed.

Because the parameter of interest is thermal conductivity and not temperature distribution, there is no need to analytically solve the steady-state equation. The value of thermal conductivity can be determined via knowledge of the applied heat flux, q/A, the thickness of the components, x, the convective heat transfer coefficient, h, and the temperature difference across the specimen, ΔT , through utilization of the series resistance concept:

$$\frac{\mathbf{q}}{\mathbf{A}} = \frac{(\Delta T)}{\left[\left(\frac{\mathbf{x}}{\mathbf{k}} \right)_{Al} + \left(\frac{\mathbf{x}}{\mathbf{k}} \right)_{PVC} + \left(\frac{\mathbf{x}}{\mathbf{k}} \right)_{Paste} + \left(\frac{\mathbf{x}}{\mathbf{k}} \right)_{Fluid} + (1/h) \right]}$$
[4.14]

Calculation of the thermal conductivity of the ER fluid, using a value of 5 W/m²K for h, resulted in a reproducible value of 0.2 W/mK. The limits on accuracy are related to the lack of knowledge about the convective heat transfer coefficient. The thermal conductivity measured was an effective value, as in the transient case. This method gave reasonable agreement with the value of thermal conductivity obtained from the transient measurements for isotropic suspensions. When low voltage fields were applied to the ER sample, the amplifier current- limited almost immediately. The steady-state temperature in the system upon application of the field was near 60°C, considerably higher than the maximum temperature reached for the transient measurements. The current generations were observed to increase dramatically with temperature of the composite specimen. These temperature-sensitive current generations, as monitored via the front panel of the supply/amplifier, rendered the application of any finite amount of electric field impossible.

Chapter 5

Conclusions and Recommendations

The short experimental times in the 1-D transient heat conduction analyses minimized the error due to heat losses versus typical steady-state experiments. Information about both thermal conductivity and specific heat were extracted from a single experiment. Extra care had to be taken in electrically insulating the thermocouples to prevent noise in the measurements due to application of electric fields, which complicated the Prop-1D model. This insulation also imposed a constraint on sensor location, in turn limiting the experimental optimization. Although some degree of precision was sacrificed, evaluation of thermal properties in DC field environments was possible.

Agreement with literature values for silicon oil and water were within 8 % for thermal conductivity and 13% for volumetric specific heat. Replicate measurements were in agreement to within 4% and 8% for thermal conductivity and volumetric specific heat, respectively. Replicate measurements of the thermal properties of the ER fluids prior to application of electric fields gave estimates within 3% of one another. Evaluation of the sensitivity coefficients and residuals for all of the materials analyzed revealed correlated

Although the experiment was not ideal, the values obtained for thermal conductivity were reproducible and in reasonable agreement with literature values. The results obtained for volumetric specific heat measurements were less reliable, but too were reproducible. Although there were some challenges with utilizing the 1-D transient heat conduction experiment, the method seemed able to predict values with enough precision to be utilized for evaluating property changes above the limit imposed by the typical spread about the mean.

At low field strengths no statistically significant change in thermal properties was observed. Based on the electrical behavior during these experiments and similar experimentation with the microscopic imaging apparatus, it seems likely that chaining is indeed occurring at these field strengths.

The application of higher field strengths was not possible due to the bounds imposed by the current limit of the high voltage power supply (5 mA) and the inherent electrical conductivity of the ER fluid composite. Because the current levels that were generated upon application of field strengths on the order of 500V/mm exceeded 5 mA, high voltage levels could not be sustained. This power consumption was a problem, not only limiting the voltage range in which measurements could be taken but possibly excluding the voltage levels necessary for sufficient chaining activation. Depending on the sensitivity of the fluid (a direct consequence of its water content), the high voltage limit before substantial heating occurred was generally in the range of 300-500 V/mm.

Steady-state methods proved to be equally disadvantageous. Higher temperatures were necessitated for these experiments and thus the challenges of minimizing the current were magnified.

There are several routes to minimizing the current generation such that this generation term can be neglected. Precise control of the conductivity of the ER fluid via control of the moisture content could be a viable alternative for the system explored in this work. This would require the utilization of environmental chambers or similar equipment to precisely and reproducibly manipulate the water content. Another route to minimize the problems associated with high conductivities would be to select new materials which have more stringently controlled electrical properties. The utilization of AC fields, although proffering its own challenges in terms of insulating thermocouples from induced noise, would likely not have the same problems with heat generation due to currents, as the sinusoidal current density averages to zero.

From the transient measurements it was evident that the thermal conductivity of the ER fluids increased with increasing volume concentration of fluid. The presence of the zeolite insulating particles thus served to augment the effective thermal conductivity instead of decrease it. This complicates the ability to predict the effect of ER fluid chaining on the value of effective thermal conductivity.

Within the voltage limits imposed by minimal current generation, a change in effective thermal conductivity was not be observed for the range of volume fractions investigated. Although the primary focus should be to isolate the conductivity regime which allows for maximum application of voltage without substantial current generation,

advances towards effective heat transfer augmentation can also be made via control of fluid design parameters. Although the transition from an isotropic to a chained structure in ER fluids should yield changes in effective thermal conductivity, based on the results of Furmanski and Floryan (1994) it stands to reason that utilizing particles with an aspect ratio greater than 1.0 (spherical) should substantially increase the dynamic range over which these particles operate.

The non-linearity of the effective thermal conductivity with particle concentration complicates the explanation of observed results. To further optimize the methodology it would seem desirable to utilize a disperse phase that is non-porous in nature. The simplest choice would be a material with a thermal conductivity of several orders of magnitude larger than the suspending medium. This would serve to simplify the expression for effective thermal conductivity and possibly permit examination of the effect of ER chaining on the thermal properties of the individual phases. This in turn would lead to a greater understanding of the overall effect on the heat transfer occurring in ER fluid composites.





Appendix A Fundamental Issues

A.1 Inter-particle Forces

To address the underlying science of ER phenomena, it is necessary to first define the regime within which these materials lie. The term 'suspension' is often used generically to describe a mixture of finely divided solid particles within a gas or liquid medium. By definition, however, for such a dispersion to be deemed a suspension, the solid phase must spontaneously settle (Brady & Holum, 1993). The dimensions of the suspended phase, as well as the densities of both the suspended phase and the suspending medium will determine the rate of this settling. A 'solution' differs from a suspension in that the dispersed phase involves molecules (Everett, 1988). The molecules resist settling because of thermal motion. Intermediate to these regimes are the colloids, wherein the dispersed phase has dimensions in the range of 1-500 nano-meters (Weiser, 1949). The particles in colloids do not settle, diffuse very slowly, and have very large surface areas relative to particle volume. Although the bulk of ER fluids are technically suspensions due to the size of the suspended particles, there are materials that push over into the colloidal and solution regimes and still demonstrate an ER response (Filisko, 1994).

The ER fluid investigated in this work, as well as many of the ER fluids discussed in the literature (Uejima, 1972; Conrad, 1994; Kordonsky et al., 1991), have particle dimensions on the order of micrometers, and may border on the edge of the colloidal domain. Because the implementation of a disperse phase of colloidal dimensions would circumvent the need to address settling issues in ER fluid-filled composites, it would seem desirable to push this dimensional envelope. The field of colloidal science intrinsically imparts much to the quest for an understanding of the ER fluid phenomenon.

Shown in Figure A1 is type 3A zeolite, an open framework aluminosilicate that has the general formula M_y [(SiO₂)_x (AlO₂)_y]• n H₂O. It was used as the disperse phase in the ER fluids investigated in this study. The framework is made up AlO₄ and SiO₄ tetrahedra, which share apical oxygens, giving rise to a 3-dimensional crystal lattice called a sodalite or β cage. When these sodalite cages are stacked together, large cavities form, and these internal volumes are connected to one another through pores or apertures. This results in an ordered cubic array of channels with precise diameters. These highly porous structures yield surface areas in the range of 300-700 m²/g, with 98% of the surface area being internal. The pore size in a typical type 3A zeolite is approximately 3.5 Angstroms, which is large enough to permit the penetration of water molecules and small ions.

The sodalite cage has a net negative charge. This negative charge is balanced by Na⁺ cations. The Na⁺ ions in the beta cages are held by electrostatic attraction to the oxygen anions in the framework (Dean, 1948). When the zeolite is fully water-loaded the Na⁺ ion can exchange for other cations in the water.

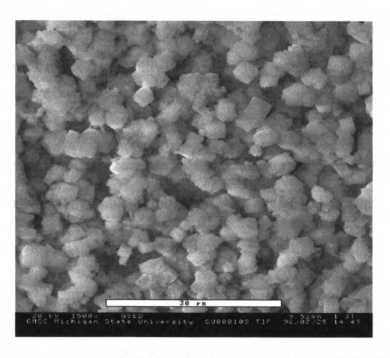


Figure A.1 Environmental Scanning Electron Microscopy (ESEM) image of UOP Type 3A zeolite in a minimum amount of silicon oil.

To formulate theoretical models to predict electrorheological response and design materials tailored to specific applications, it is necessary to understand the long-range and short-range inter-particle forces leading to suspension stability, and the ER effect in general. These molecular forces can be characterized in terms of interactions between fluctuating dipoles and motions of outer electrons, and can be calculated quantum mechanically. A summary of these calculations as outlined by Everett (1988) follows.

Attractive forces are quantified as:

$$\mathbf{F}^{\mathsf{aff}} = \frac{-\mathbf{A}}{\mathsf{r}^7} \tag{A.1}$$

It can be seen that the attractive force increases in magnitude as the molecules approach one another. At nuclei separation r, this force is proportional to the inverse seventh power of separation. From this, the free energy of attraction between a pair of atoms or molecules from a distance d to infinity can be found by integration, yielding:

$$\Delta G^{att} = \frac{-A'}{d^6}$$
 [A2]

A' can be expressed roughly in terms of experimental quantities that are related to the nature of the individual molecules through quantum mechanical properties:

$$A' = (3/4)hv\alpha^{2}$$
 [A3]

where,

h = Plank's Constant (6.63 E-34 Js)

v = a characteristic frequency associated with the first ionization energy

 α = polarizability

For two dissimilar molecules, 1 and 2:

$$A'_{12} = (3/2)h\left(\frac{v_1v_2}{v_1 + v_2}\right)\alpha_1\alpha_2$$
 [A4]

So, as the atoms approach, the free energy becomes increasingly negative, because of the increasing attractive force. At close distances however, the electron clouds begin to interact and if the electrons are in non-bonding orbitals, repulsive forces arise. This causes the free energy to rise. When the electron clouds interpenetrate this free energy becomes essentially infinite. This is referred to as Born Repulsion, and gives rise to the approximate expression for free energy of repulsion:

$$\Delta G^{\text{rep}} = \left(\frac{\mathbf{B'}}{\mathbf{d}^{12}}\right)$$
 [A5]

The total potential energy, referred to as the Lennard-Jones potential, is thus given by:

$$\Delta G = \Delta G^{\text{rop}} + \Delta G^{\text{att}} = \left(\begin{array}{c} B' \\ \overline{d}^{12} \end{array} \right) + \left(\begin{array}{c} -A' \\ \overline{d}^{6} \end{array} \right)$$

Usually the depth of the potential well, ε_{min} , is a more convenient measure of the interaction than the constants A' and B'. The expression thus becomes:

$$\Delta G = 4\varepsilon_{\min} \left[\left(\frac{r_o}{d} \right)^{12} - \left(\frac{r_o}{d} \right)^{6} \right]$$
 [A6]

where r_0 is the distance at which the potential is zero.

What we have arrived at is a description of the free energy interaction of two molecules. To determine inter-particle relationships it is necessary to find a model which accurately accounts for the interactions between all molecules in all particles within the limits of influence of the individual forces.

Halsey (1992) has experimentally studied the long-range, anisotropic character of the forces attributing to electrorheological response. Ginder (1993) has also studied interparticle interactions using non-invasive diffuse optical probes to elucidate time scales for structure formation. These results compared favorably with predictions based on dielectric properties.

A.2 Dielectric Phenomenon

In Winslow's original work (1949) he alluded to the role of dielectric properties in ER activity. Many researchers since have elaborated upon these precepts to generate comprehensive models of the ER effect that detail the relationship between the dielectric

constants of the disperse phase and the suspending medium. (Davis, 1992a; Khusid, 1996). This interplay of properties has been indicated as an important criterion in developing materials with an ER response. In a recent finite element model by Davis (1992b) it was shown that ER response depends on different dielectric properties depending on the field conditions. At high frequencies it was found that the dielectric mismatch was the dominant parameter in determining the capacity for ER behavior, whereas at low frequency and D.C. field conditions the ratio of particle to suspending medium electrical conductivities was a controlling factor. These results were based on a dipole approximation.

A dielectric is an insulating material having distinct electrical properties, in that it can carry energy by way of a charge separation. Polar molecules, which possess a permanent charge separation, and non-polar molecules, which develop induced dipole moments when subjected to an external electric field, are both considered dielectrics. Polar molecules are characterized by the presence of permanent dipole moments, in association with charges -q and +q being separated by a distance d:

$$\mu = q d$$
 [A.7]

The magnitude of the dipole moment depends on the size and symmetry of the molecule (Hill et al., 1969). Although a symmetrical molecule may have no permanent polarization, a temporary dipole can be induced by the application of an external field, E_o (Serway, 1986). This causes the centers of positive and negative charges to shift to opposite sides of the molecule. The result is an induced surface charge density, σ_i , on the one face of the particle, and an equal negative surface charge density on the opposite face, as is illustrated in Figure A.2. In Type 3A zeolite, the positive Na⁺ ions would migrate (within the zeolite

framework) towards the negative electrode, resulting in a net positive charge on one side of the particle and a net negative charge on the other due to the anionic framework.

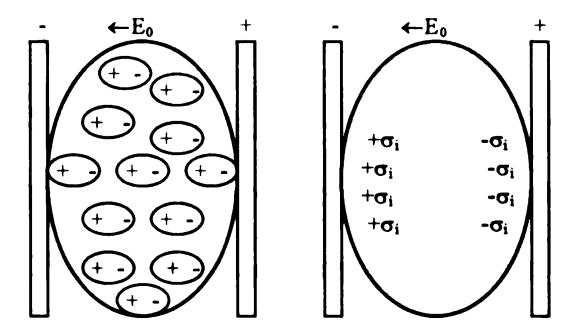


Figure A.2 Conceptualization of a dielectric particle experiencing a charge separation due to an applied electric field E_0 . (a) The centers of positive charge in the dielectric particle (Na⁺ ions in zeolites) shift towards the negative electrode, and the centers of negative charge shift towards the positive electrode (b) The result is a net positive surface charge on the one side of the particle and a net negative charge on the other.

An opposing electric field E_1 is induced as a direct result of these newly developed surface charges. The net electric field is thus given by the added effects of these opposing fields:

$$\mathbf{E} = \mathbf{E}_{\mathbf{a}} - \mathbf{E}_{\mathbf{t}}$$
 [A.8]

The applied field, E_0 , is reduced by a factor κ , in the presence of a dielectric, yielding the net electric field E:

$$\mathbf{E} = \frac{\mathbf{E}_{\bullet}}{\kappa}$$
 [A.9]

κ is a property of the material and is called the dielectric constant. Related to dielectric constant is the dielectric strength of the material. This represents the maximum electric field that can be applied before the material breaks down electrically. The manufacturer lists silicon oil as having a dielectric strength of 350 V/mil, and a dielectric constant of 2.95. Water has a dielectric constant of 80.

There are three effects giving rise to the total polarizability, α_T , of a molecule and thus we sub-classify polarization as being either electronic, α_e , atomic, α_e , or orientational, α_o . In non-polar molecules the latter effect is not present. These different types of polarization are shown below in Figure A.3. Electronic polarization, the biggest contributor, is induced by the displacement of atoms relative to the nucleus of each atom. The displacement of the atomic nuclei relative to each other renders atomic polarization. These two types combined are called distortion polarization. Orientation polarization occurs only in polar molecules. In the absence of a field, the permanent dipole moments are randomly distributed and are constantly changing direction as a result of thermal motion. The application of a field causes alignment, giving rise to orientation polarization. This additional polarization typically gives polar molecules higher permittivities. Orientation polarization drops off rapidly as the temperature increases and thermal motion tends to disrupt the alignment.

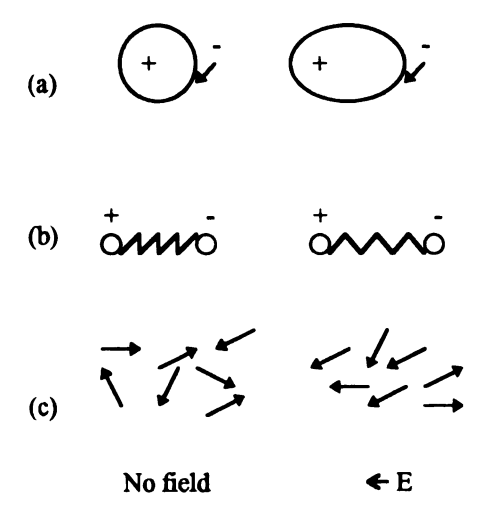


Figure A.3 Types of polarization mechanisms observed in non-polar molecules (von Hippel, 1995):(a)electronic (b)atomic (c)orientation

The permittivity of an isotropic material is given in terms of the polarization P produced by an applied field E_0 :

$$\varepsilon_{0} = 1 + \frac{4 \pi P}{\varepsilon E_{0}}$$
 [A.10]

where ε is a constant that depends on the system of units being used. The induced surface charge density (or induced electric moment per unit volume) can be represented by:

$$\mathbf{P} = \mathbf{N}_1 \mathbf{m} \tag{A.11}$$

where N_1 is the number of molecules per unit volume and \mathbf{m} is the average induced moment due to all types of polarization. If we denote the average field acting on a molecule as \mathbf{F} then we may write:

$$\mathbf{m} = \boldsymbol{\alpha}_{\mathsf{T}} \mathbf{F} \tag{A.12}$$

where α_T is given by:

$$\alpha_{\rm T} = \alpha_{\rm e} + \alpha_{\rm a} + \alpha_{\rm o} \tag{A.13}$$

The relative permittivity can thus be written as:

$$\varepsilon_0 = 1 + \frac{4\pi N_1 \alpha_T F}{E_2 \varepsilon}$$
 [A.14]

The three types of polarizability respond differently to the frequency of the applied field. At low frequencies all types of polarization can reach their corresponding steady field value. With increasing frequency the limits of response time are reached. Orientation polarization is the first to be affected. It contributes less and less as the frequency rises. The fall of total polarizability from

$$\alpha_{\rm T} = \alpha_{\rm e} + \alpha_{\rm e} + \alpha_{\rm o} \tag{A.15}$$

$$\alpha_{\rm T} = \alpha_{\rm e} + \alpha_{\rm e} \tag{A.16}$$

as well as the associated drop in permittivity, is referred to as the dielectric dispersion. Because the time scale for electronic and atomic polarization is so short, in the frequency range of the dielectric dispersion the distortion polarization remains unchanged. However, at frequencies comparable to the natural frequencies of the vibrations of the atoms in the molecules, $\alpha_{\rm e}$ will fall off much more quickly than $\alpha_{\rm e}$ and another dispersion will occur. This typically occurs in the infrared region. The electronic polarization will reach its response limit at frequencies corresponding to the electronic transitions between different atomic energy levels. These are typically in the visible, ultra-violet, and X-ray regions of the spectrum.

Knowledge of the dielectric dispersion can thus help to elucidate many questions regarding the molecular mechanisms responsible for bulk properties in ER fluids. Atomic, electronic, and orientational effects are directly attributable to molecular structure, and thus information regarding these contributions service the molecular design of advanced electrorheological materials. It is also here in the realm of dielectric dispersions that models of electrorheological based on interparticle forces coalesce with trends observed via measurement of dielectric properties.

Investigation of measured dielectric property dependences is a very instructive means of elucidating the nature of ER response. It is an alternative to studying interparticle forces but complements this body of information well. Instead of dealing with the individual forces of attraction and repulsion and from there synthesizing a net response to externally applied fields, the ER response is tied to properties such as conductivity,

dielectric strength, and permittivity. Inherent to both descriptions is the nature of the polarizability of the particles in suspension. Although the approaches are different they are founded on the same phenomenon.

A.3 Interfacial Electric Double Layer Theory

Although the ER response is generally attributed to the polarization of particles under an applied electric field, this description does not account for the fact that not all particles with a high permittivity demonstrate an ER effect (Filisko,1994), nor does it account for the speed of the chaining response (Uejma, 1972). Klass and Martinek (1967ab) observed ER activity at high frequency AC fields where chain reforming based on particle polarization alone seemed kinetically unlikely. Theories on electric double layers for electrolytic suspensions have been around since the beginnings of colloidal science (Graham, 1861) although Schwartz (1962) was the first to propose the electric double layer as a mechanism for the ER response in non-conducting suspending media. Since then, this theory has gain prominence in many theories based on dielectric phenomena (Khusid, 1996).

Fundamental to the development of an electric double layer is the presence of electrical charges on the surface of the suspended particles. These charges may arise from several different mechanisms, including ionization of surface molecules, differential solution of ions from the surface of the particle, isomorphous substitution, and preferential ion adsorption (Everett, 1988; Weiser, 1949). Selective adsorption of H+ and OH- ions from water may also contribute to the formation of charged surfaces. In zeolites it is generally believed that the adsorbed layer is H₂O (Uejima, 1972). The electrical charge at

the particle surface due to the adsorbed species attracts a layer of oppositely charged ions. The combination of these negatively and positively charged layers is referred to as the electric double layer. When the electric charge in one of these layers is diffusely distributed, the assemblage is referred to as a diffuse double layer. Electric double layers have been well characterized for aqueous electrolytic solutions however the characterization of the nature of the double layer in nonageous/nonpolar systems (which include ER systems) is complicated by the lack of a clearly identifiable ionic species (Kitahara and Watanabe, 1984). Water is present in most ER fluids, although the amount is small and also difficult to control. Water has the potential to deplete electrons in the suspending hydrocarbons resulting in free ions which could contribute to proton conductivity, hence it may play a key role in the establishment of diffuse double layers. The development of anhydrous systems by Block and Kelly (1988) has raised new questions and perhaps closed old ones regarding the role of water in ER response. Much is still not clearly understood however.

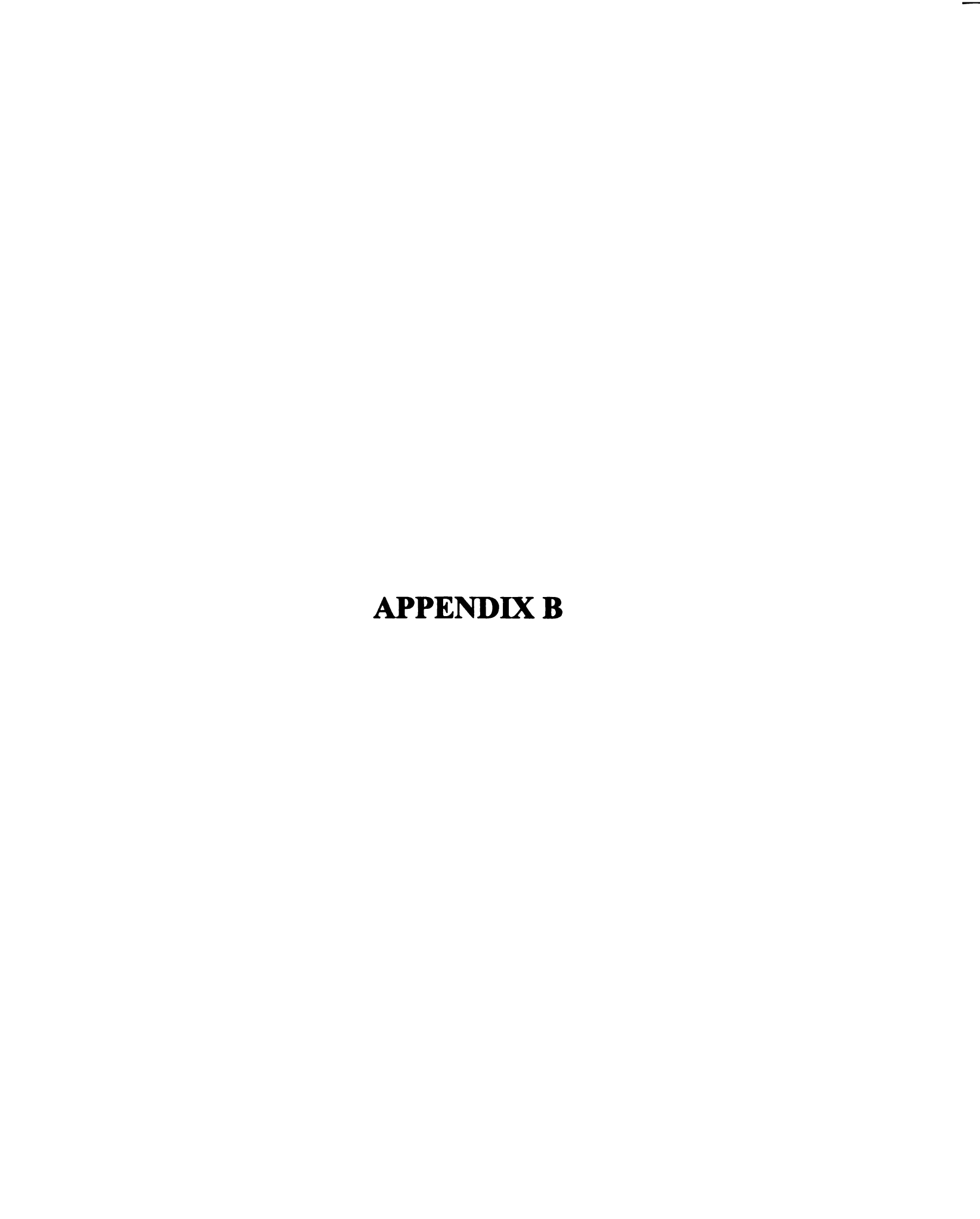
The measurement of dielectric dispersions is becoming increasingly important in evaluating double layer theories and understanding the molecular mechanisms associated with this response. Although ER response is generally attributed to the polarization of particles under an applied field, it is difficult to predict ER activity based solely on the polarizability of the suspended phase. Polar materials possessing permanent dipoles have high orientational polarizability and thus high permittivities, yet are not ER active.

Uejima (1972) proposed a dielectric model to explain the speed of chaining response in ER systems. His results demonstrated the applicability of electric double layer theory. He found the particle surface charge density to be closely related to the fraction of

adsorbed water in the ER system and theoried that the adsorbed water layer directly affects the surface charge density of the electric double layers, and also increases the dielectric constant of the ER fluid. The observed Winslow effect increased accordingly. He also observed that when the particles were completely dried, electric double layers never seemed to form because of the absence of dielectric dispersions at low frequencies. There was also no evidence of an ER effect for dry fluids.

Filisko (1994), in an examination of four different types of ER fluids, found that the presence of a unique dielectric dispersion is linked to ER activity. Although these results do not conclusively point to a specific molecular 'mechanism' that can be deemed responsible for the ER effect, they do indicate the underlying molecular 'features' that are critical to the ER response. This is valuable information for designing ER fluids with enhanced reactivity.

To bring this discussion full circle, the permittivity of a material is a quantification of its polarizability with respect to a given applied field. The polarizability of a molecule represents the interplay of molecular forces at work in the material of interest and the dipole moments that are set up due to applied fields. Although high permittivities are needed to manifest electrorheological behaviour, this is a necessary, but not sufficient characterization. Electric double layer theory attempts to complete this description by bringing into play the effects of surface charge and density, and its role in the interaction of the disperse phase and its suspending medium.



Appendix B Triple Junction Thermocouples

The Copper-Constantan triple-junction thermocouples are parallel thermocouple constructions, outputting the average temperature of three junctions. This type of circuit yields a true arithmetic average of the of the individual thermocouples if all of the thermocouple circuits are of equal resistance (ASME, 1974). In the experiments in this work, the temperature at each of these junction locations was essentially equivalent as heat flow in the transverse direction was negligible. This had been confirmed experimentally via observation of a spatial distribution of thermocouples. The typical configuration of parallel junction thermocouples (Beckwith et. al., 1982) is shown in Figure B1(a). Based on the Law of Intermediate Metals for thermocouples, the sequence of constructions shown in Figure B1(b) through (d), are equivalent to the configuration shown in Figure B1 (a), as long as T(ref.) remains constant. The configuration used in this work is best understood in terms of Figure B1 (d).

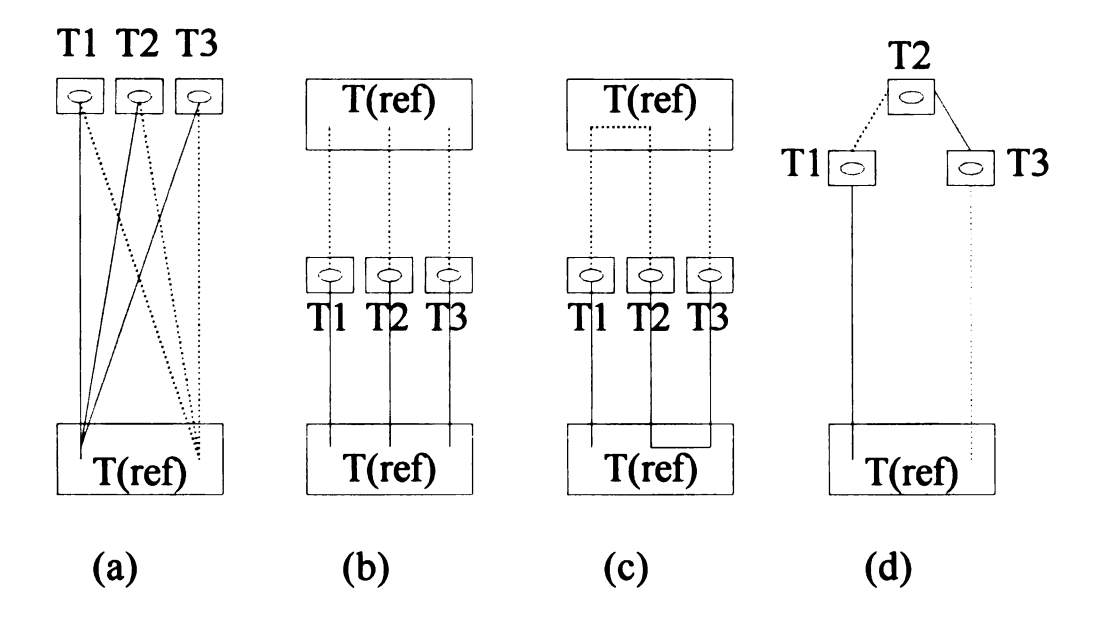


Figure B.1 Construction of parallel 3 junction thermocouples: (a) typical construction (b) - (d) electrically equivalent constructions based on the Law of Intermediate Metals for thermocouples.

APPENDIX C	

r

Ļ

Appendix C Q-Basic Program for Temperature Data Conversion

5 Interval=0 10 Open "C:\star\test.dat" For INPUT as #1 Open "C:\elliott\Ze 15.txt" For OUTPUT as #2 20 25 IF EOF(1) THEN 80 INPUT #1, time, voltage, t2, t3, t4, t5, t6, t7, t8, t9, t10, t11, t12, t13, t14, 50 t15, t16, t17, t18, t19, t20, t21, t22, t23 WRITE #2, time, t2, t3 60 70 **GOTO 25** Close #1, #2 80 **End** 90

APPENDIX D

Appendix D PROP-1D Sample Data Files

The sample data files that follow include an input control parameter file (*.icp), a data file containing the heat flux data and the experimental temperature profiles (*.txt), and an output file (*.out) which is generated by the PROP-1D program.

FILE: vf15_2Licp

BLOCK 1 : HEADER

15% vol fraction Zeolite/Silicon Oil/Test 2/ Aug. 14th,1996

BLOCK 2: GEO R1 NREG ITER ICONVR IPRINT ISTOR IDTAIL .00 1.00000 7 8 0 0 1

BLOCK 3: INDICES FOR SIDE HEAT LOSS (I.E., FIN)

DIMENS GEO2ND HSIDE DSIDE TINF 1.00000 .00000 .00000 1.00000 .00000

BLOCK 4: MAT(IA),IA=1,NREG (Material numbers for regions)
1 2 3 4 5 4 3

BLOCK 5: TL(IB),IB=1,NREG (Thicknesses for regions) 0.00014 0.00034 0.00016 0.00075 0.003 0.00075 0.00016

BLOCK 6: MN(IC),IC=1,NREG (Number nodes for regions) 3 3 5 3 25 3 5

BLOCK 7: ICAL TTSTAT IQINT TIMON TIMOF 4 0.0000 1 600.0000 750.0000

BLOCK 8: TIMREG(IC),IC=1,NTMREG (Time regions)
123

BLOCK 9: BOUNDARY CONDITION INDICES [T IS 1, Q IS 2]

IBCXZ IXZVAR IBCXL IXLVAR

2 1 2 0

BLOCK 10: DATA FILE INDICES NTIM NCOLM IDATA 42 3 0

BLOCK 11: ITORQ(IQ),IQ=1,NCOLM (Temperature or heat flux index)
2 1 1

BLOCK 12: INTFAC(IQ),IQ=1,NCOLM (Interface index, 0 for x=0 surface) 0 2 7

BLOCK 13: WTING(IQ),IQ=1,NCOLM (Weights) 1.0 1.0 1.0 1.0

- BLOCK 14: NKTEMP(I) NCTEMP(I) (No. k & rho*c s)
 1 1
- BLOCK 15: TEMPERATURE THERMAL COND. 0.000 0.980
- BLOCK 16: TEMPERATURE VOL HEAT CAP.

0.000 1871000

- BLOCK 14: NKTEMP(I) NCTEMP(I) (No. k & rho*c s)

 1 1
- BLOCK 15: TEMPERATURE THERMAL COND. 0.000 2.307
- BLOCK 16: TEMPERATURE VOL HEAT CAP. .000 1369000
- BLOCK 14: NKTEMP(I) NCTEMP(I) (No. k & rho*c s)

 1 1
- BLOCK 15: TEMPERATURE THERMAL COND. 0.000 0.168
- BLOCK 16: TEMPERATURE VOL HEAT CAP. .000 1334400
- BLOCK 14: NKTEMP(I) NCTEMP(I) (No. k & rho*c s)

 1 1
- BLOCK 15: TEMPERATURE THERMAL COND. 0.000 167.27
- BLOCK 16: TEMPERATURE VOL HEAT CAP. .000 2463000

BLOCK 14: NKTEMP(I) NCTEMP(I) (No. k & rho*c s)
1 1

BLOCK 15: TEMPERATURE THERMAL COND. 0.000 0.1461

BLOCK 16: TEMPERATURE VOL HEAT CAP. .000 2345000

BLOCK 17: NUMK NUMC IWEIGH ISEQU IREGUL 1 1 0 0 0

BLOCK 18: IPK(mat.) JPK (index) (k indexes)
5 1

BLOCK 19: IPC(MAT.) JPC (INDEX) 5 1

FILE: vf15_2.txt

0	24.6001	24.5589
0	24.6046	24.6046
0	24.6071	24.6071
0	24.5871	24.5871
0	24.586	24.586
1894	26.7055	24.6061
1894	28.4887	24.6058
1894	29.98	24.6055
1894	31.06	24.6261
1894	32.0806	24.6505
1894	33.0988	24.7571
1894	34.1111	24.8804
1894	34.937	25.0628
1894	35.8069	25.2504
1894	36.5939	25.4369
1894	37.4533	25.6782
1894	38.1444	25.9129
1894	38.864	26.1982
1894	39.5236	26.4845
1894	40.2677	26.7761
1894	40.8696	27.0455
1894	41.5245	27.3701
1894	42.1602	27.696
1894	42.8156	28.0428
1894	43.3519	28.3494
1894	43.9475	28.6766
1894	44.5226	29.024
1894	45.1198	29.3946
1894	45.6332	29.6996
1894	46.1356	30.0547
0	44.944	30.397
0	43.4603	30.7682
0	42.6425	31.0913
0	41.9241	31.4154
0	41.3102	31.7247
0	40.7356	32.0339
0	40.2965	32.2578
0	39.8718	32.456
0	39.5289	32.5954
0	39.1301	32.7392
0	38.8273	32.8384
0	38.5051	32.9385
	0 0 0 1894 1894 1894 1894 1894 1894 1894 1894	0 24.6046 0 24.6071 0 24.5871 0 24.586 1894 26.7055 1894 28.4887 1894 29.98 1894 31.06 1894 32.0806 1894 33.0988 1894 34.1111 1894 35.8069 1894 36.5939 1894 37.4533 1894 37.4533 1894 38.864 1894 39.5236 1894 40.2677 1894 40.2677 1894 42.1602 1894 43.3519 1894 43.9475 1894 45.6332 1894 45.6332 1894 45.6332 1894 45.6332 1894 45.6332 1894 45.6332 1894 45.6332 1894 45.6332 1894 46.1356 0 40.26425 0 41.9241

FILE: vf15 2 O.out

PROGRAM PROPID

Version 5.31 November 1993

Written by James V. Beck

Beck Engineering Consultants Company

Ph: 517-349-6688

NAME OF FILE OF INPUT CONTROL PARAMETERS:

vfl 5-2i.icp

NAME OF FILE OF EXPERIMENTAL DATA:

vf15-2.txt

NAME OF OUTPUT FILE:

vf15-2-O.out

BLOCK 1: HEADER

BLOCK 1 : HEADER

BLOCK 2: GEO R1 NREG ITER ICONVR IPRINT ISTOR IDTAIL

.00 1.00000 7 8 0 0 1

Since ICONVR = 0, the units must be consistent.

BLOCK 3: INDICES FOR SIDE HEAT LOSS (I.E., FIN)

DIMENS GEO2ND HSIDE DSIDE TINF

1.00000 .00000 .00000 1.00000 .00000

BLOCK 4: MAT(IA), IA=1, NREG (Material numbers for regions)

1 2 3 4 5 4 3

BLOCK 5: TL(IB), IB=1, NREG (Thicknesses for regions)

.00014 .00034 .00016 .00075 .00300

.00075 .00016

BLOCK 6: MN(IC),IC=1,NREG (Number nodes for regions)

3 3 5 3 25 3 5

BLOCK 7: ICAL TTSTAT IQINT TIMON TIMOF

4 .0000 1 600.0000 750.0000

BLOCK 8: TIMREG (End of time region)

123.00

BLOCK 9: BOUNDARY CONDITION INDICES [T IS 1, Q IS 2]

IBCXZ IXZVAR IBCXL IXLVAR

2 1 2 0

BLOCK 10: DATA FILE INDICES NTIM NCOLM IDATA 42 3 0

BLOCK 11: ITORQ(IQ),IQ=1,NCOLM (Temperature or heat flux index)

2 1 1

BLOCK 12: INTFAC(IQ),IQ=1,NCOLM (Interface index, 0 for x=0 surface)
0 2 7

BLOCK 13: WTING(IQ),IQ=1,NCOLM (Weights)
1.0 1.0 1.0

BLOCK 14: NKTEMP(I) NCTEMP(I) (No. k & rho*c s)
1 1

BLOCK 15: TEMPERATURE THERMAL COND. .000 .980

BLOCK 16: TEMPERATURE VOL HEAT CAP. .000 1871000.000

BLOCK 14: NKTEMP(I) NCTEMP(I) (No. k & rho*c s)
1 1

BLOCK 15: TEMPERATURE THERMAL COND. .000 2.307

BLOCK 16: TEMPERATURE VOL HEAT CAP. .000 1369000.000

BLOCK 14: NKTEMP(I) NCTEMP(I) (No. k & rho*c s)
1 1

BLOCK 15: TEMPERATURE THERMAL COND. .000 .168

BLOCK 16: TEMPERATURE VOL HEAT CAP. .000 1334400.000

BLOCK 14: NKTEMP(I) NCTEMP(I) (No. k & rho*c s)
1 1

BLOCK 15: TEMPERATURE THERMAL COND. .000 167.270

BLOCK 16: TEMPERATURE VOL HEAT CAP. .000 2463000.000

BLOCK 14: NKTEMP(I) NCTEMP(I) (No. k & rho*c s)
1 1

BLOCK 15: TEMPERATURE THERMAL COND. .000 .146

BLOCK 16: TEMPERATURE VOL HEAT CAP. .000 2345000.000

BLOCK 17: NUMK NUMC IWEIGH ISEQU IREGUL 1 1 0 0 0

BLOCK 18: IPK(mat.) JPK (index) (k indexes)
5 1

BLOCK 19: IPC JPC 5 1

END OF THE INPUTS

NNN 47

ITER RMS TH. COND. RHO SPHT. DEL-K DELCP

0 .518 .1601 .2298E+07 .1E-01 -.5E+05

1 .363 .1611 .2298E+07 .1E-02 -.2E+03

2 .362 .1611 .2298E+07 .2E-04 -.1E+03

TIME TH. COND. VOL. HEAT

3.00 .1611E+00 .2298E+07

6.00 .1611E+00 .2298E+07

9.00 .1611E+00 .2298E+07

12.00 .1611E+00 .2298E+07

15.00 .1685E+00 .2375E+07

18.00 .1735E+00 .2426E+07

```
21.00
        .1636E+00 .2322E+07
24.00
        .1582E+00 .2261E+07
27.00
        .1565E+00 .2230E+07
30.00
        .1571E+00 .2174E+07
33.00
        .1595E+00 .2081E+07
36.00
        .1661E+00 .1985E+07
39.00
        .1711E+00 .1910E+07
42.00
        .1736E+00 .1883E+07
45.00
        .1743E+00 .1865E+07
48.00
        .1744E+00 .1873E+07
51.00
        .1744E+00 .1884E+07
54.00
        .1744E+00 .1900E+07
57.00
        .1738E+00 .1916E+07
60.00
        .1731E+00 .1939E+07
63.00
        .1725E+00 .1960E+07
66.00
        .1719E+00 .1979E+07
69.00
        .1713E+00 .1995E+07
72.00
        .1707E+00 .2015E+07
75.00
        .1701E+00 .2034E+07
78.00
        .1696E+00 .2053E+07
81.00
        .1690E+00 .2068E+07
84.00
        .1684E+00 .2087E+07
87.00
        .1679E+00 .2105E+07
90.00
        .1662E+00 .2105E+07
93.00
        .1654E+00 .2118E+07
96.00
        .1648E+00 .2133E+07
99.00
        .1643E+00 .2150E+07
102.00
         .1639E+00 .2168E+07
105.00
         .1636E+00 .2186E+07
108.00
         .1632E+00 .2204E+07
         .1628E+00 .2222E+07
111.00
114.00
         .1624E+00 .2241E+07
117.00
         .1620E+00 .2260E+07
120.00
         .1615E+00 .2279E+07
123.00
         .1611E+00 .2298E+07
```

CALCULATED T(I,J) = ETEMP(I,J) - DTETC(I,J)

```
TIME
        ETEMP
                   DTETC
                            STRMS (k*dT/dk) (c*dT/dc)
3.00
       24.605
                .011
                       .011 -.136E-02 -.425E-03
                .039
                       .039 .170E-02 .261E-03
3.00
       24.605
6.00
       24.607
                .014
                       .013 -.227E-02 -.369E-03
6.00
       24.607
                .040
                       .039 .256E-02 .353E-04
9.00
       24.587
               -.005
                       .011 -.299E-02 -.201E-03
9.00
       24.587
                .018
                       .034 .330E-02 -.281E-03
```

```
12.00
         24.586
                  -.005
                          .010 -.360E-02 .120E-05
12.00
         24.586
                   .016
                          .030 .395E-02 -.625E-03
15.00
         26.705
                  -.566
                           .253 -.949E-01 -.971E-01
15.00
         24.606
                   .036
                          .032 .452E-02 -.958E-03
18.00
         28.489
                  -.157
                          .240 -.321
                                        -.325
18.00
         24.606
                   .034
                          .032 .585E-02 -.204E-02
21.00
         29.980
                   .130
                          .227 -.583
                                       -.587
21.00
         24.605
                          .032 .170E-01 -.119E-01
                   .031
24.00
         31.060
                   .109
                          .216 -.858
                                       -.861
24.00
         24.626
                   .041
                          .033 .571E-01 -.475E-01
27.00
         32.081
                   .106
                          .207 -1.14
                                       -1.14
27.00
         24.650
                   .038
                          .034 .139
                                       -.120
30.00
         33.099
                   .162
                          .203 -1.42
                                       -1.42
30.00
        24.757
                   .097
                          .044 .266
                                       -.233
33.00
         34.111
                   .261
                          .209 - 1.70
                                       -1.70
33.00
        24.880
                   .146
                          .061 .432
                                       -.383
36.00
         34.937
                   .216
                          .209 -1.97
                                       -1.97
36.00
        25.063
                   .227
                          .088 .632
                                       -.565
39.00
         35.807
                   .253
                          .213 -2.25
                                        -2.25
39.00
        25.250
                   .286
                          .116 .856
                                       -.774
42.00
         36.594
                   .238
                          .215 -2.52
                                        -2.52
42.00
        25.437
                   .316
                          .140 1.10
                                       -1.00
45.00
         37.453
                   .324
                          .224 -2.79
                                        -2.78
45.00
        25.678
                   .376
                          .166 1.35
                                       -1.25
48.00
         38.144
                   .268
                          .227 - 3.06
                                       -3.04
48.00
        25.913
                   .406
                          .190 1.62
                                       -1.52
51.00
         38.864
                   .263
                          .229 - 3.32
                                        -3.30
51.00
        26.198
                   .463
                          .216 1.88
                                       -1.80
54.00
         39.524
                   .219
                          .229 -3.58
                                        -3.55
54.00
                          .241 2.15
        26.485
                   .500
                                       -2.08
57.00
         40.268
                   .278
                          .231 -3.83
                                        -3.81
57.00
         26.776
                          .263 2.41
                   .522
                                       -2.37
60.00
        40.870
                   .213
                          .231 -4.07
                                        -4.06
60.00
         27.045
                   .505
                          .280 2.68
                                       -2.67
63.00
         41.525
                   .215
                          .230 -4.31
                                        -4.30
63.00
         27.370
                   .527
                          .297 2.93
                                       -2.98
66.00
         42.160
                   .214
                          .229 -4.54
                                        -4.55
66.00
         27.696
                   .534
                          .311 3.18
                                       -3.29
69.00
         42.816
                   .244
                          .230 -4.77
                                        -4.79
69.00
         28.043
                   .549
                          .325 3.42
                                       -3.60
72.00
        43.352
                          .228 -4.98
                                        -5.04
                   .168
72.00
                          .335 3.66
         28.349
                   .510
                                       -3.91
75.00
        43.947
                   .162
                          .225 -5.19
                                        -5.28
75.00
         28.677
                   .481
                          .342 3.88
                                       -4.23
78.00
         44.523
                          .223 -5.39
                                        -5.53
                   .145
```

```
78.00
         29.024
                   .460
                          .347 4.10
                                      -4.55
 81.00
         45.120
                   .160
                          .221 -5.58
                                      -5.77
 81.00
         29.395
                   .454
                          .352 4.31
                                      -4.86
 84.00
         45.633
                   .099
                          .218 -5.77
                                      -6.02
 84.00
         29.700
                   .372
                          .353 4.51
                                      -5.18
 87.00
         46.136
                          .214 -5.94
                                      -6.26
                   .035
 87.00
         30.055
                   .333
                          .352 4.70
                                      -5.50
90.00
         44.944
                   .965
                          .274 -6.02
                                      -6.41
90.00
         30.397
                   .273
                          .350 4.88
                                      -5.82
93.00
         43.460
                   .303
                          .275 -5.95
                                      -6.43
93.00
         30.768
                   .236
                          .347 5.05
                                      -6.13
96.00
         42.643
                   .143
                          .272 -5.84
                                      -6.42
96.00
         31.091
                   .145
                          .342 5.21
                                      -6.44
99.00
                                       -6.39
         41.924
                  -.016
                          .268 -5.71
99.00
         31.415
                   .059
                          .337 5.32
                                      -6.72
102.00
         41.310
                 -.143
                           .265 -5.57
                                       -6.37
102.00
         31.725
                  -.032
                           .332 5.39
                                       -6.96
105.00
         40.736
                  -.286
                           .266 -5.42
                                       -6.34
105.00
         32.034
                  -.107
                                       -7.16
                           .328 5.40
108.00
         40.297
                  -.341
                           .268 -5.26
                                       -6.31
         32.258
                  -.245
                           .326 5.37
                                       -7.33
108.00
         39.872
                                       -6.29
111.00
                  -.419
                           .273 -5.09
         32.456
                  -.386
                           .328 5.29
                                       -7.46
111.00
114.00
         39.529
                  -.449
                           .279 -4.93
                                       -6.28
114.00
         32.595
                  -.561
                           .336 5.19
                                       -7.56
117.00
         39.130
                  -.564
                           .290 -4.76
                                       -6.27
117.00
          32.739
                  -.709
                           .350 5.06
                                       -7.64
120.00
         38.827
                   -.608
                           .302 -4.58
                                       -6.26
120.00
          32.838
                  -.879
                           .373 4.91
                                       -7.70
          38.505
                  -.695
                           .318 -4.41
                                        -6.26
123.00
          32.938 -1.027
                           .402 4.74
                                       -7.74
123.00
3 .362 .1611
                .2298E+07 .4E-06 -3.
```

REG RMS TH. C VOL.
.0 .362 .1611 .2298E+07

SPATIAL CORRELATION MATRIX FOR U
.1000E+01 .4196E+00
.4196E+00 .1000E+01

PHI MATRIX = VALID(I,J)
.4646E-01 .8350E-02
.8350E-02 .8525E-02

XTWX matrix
.44731482E+05 .35581806E-03 .35581806E-03 .30787032E-09
Inverse of XTWX matrix

```
.22563050E-04 -.26077021E+02 -.26077021E+02 .32782591E+10
```

COVARIANCE MATRIX OF PARAMETERS = P, B&A, page 248

.71254553E-05 -.24670656E+02 -.24670656E+02 .23883364E+10

APPROX. SQUARE REGION CONFIDENCE REGIONS

PARAMETERS plus and minus the below values

.60861290E-02

.11142499E+06

INVERSE OF COV MATRIX OF PARAS = P INV, B&A, p 248

.14554735E+06 .15034518E-02 .15034518E-02 .43423160E-09

95.0 PERCENT B-MATRIX BECK AND ARNOLD (6.8.28) FOR COORDINATES OF (B-BETA)

B11 .1887E+01 B12 .1559E+01

B21 -.1887E+01 B22 .1559E+01

SENSOR RHO SIGMA2 FOR U AND WEIGHT USED

1.0 .6950E+00 .4646E-01 1.00

2.0 .9038E+00 .8555E-02 1.00

NEW BLOCK 21: ((XTWX(I,J),I=J,N),J=1,N), INCLUDES PRIOR INFORMATION FOR ISEQU=1

.4473E+05 .3558E-03

.3558E-03 .3079E-09

NEW BLOCK 22: ((XTPSX(I,J),I=J,N),J=1,N)

THIS IS XTWPSWX.

.1377E+05 .3217E-04

.3217E-04 .2219E-09

NORMAL TERMINATION OF PROGRAM



Appendix E Design of Experiment

E1. Sensitivity Analysis

To evaluate the suitability of the mathematical model a sensitivity analysis can be very informative. The first derivative of a dependent variable with respect to the parameter of interest is known as the sensitivity coefficient for that parameter (Beck and Arnold, 1977). The sensitivity coefficients of concern in this work are given by:

$$\frac{\partial \Gamma}{\partial k}$$
 [E.1]

and:

$$\frac{\partial \Gamma}{\partial c_p}$$
 [E.2]

If $\partial T/\partial k \sim 0$, then temperature is not very sensitive to a change in k, and to use temperature profiles to estimate k would be ineffectual. It is thus desirable to choose experimental conditions which maximize these coefficients.

Sensitivity coefficients also provide information about the linearity of the mathematical model. If the sensitivity coefficients are not functions of any of the parameters in the model then the model is said to be linear in the parameters. If the

mathematical model is non-linear in the parameters, the estimation algorithm becomes more involved. This is the case for the current problem. The sensitivity coefficients are functions of thermal conductivity and volumetric specific heat.

Sometimes it is not possible to uniquely estimate the desired parameters from a given experiment, although it may be possible to estimate a function or combination of them. This is referred to as the identifiability problem. Again examination of the sensitivity coefficients provides insight. If, over the time range of the experiment, the sensitivity coefficients are not linearly dependent, then the parameters are uncorrelated and can be estimated uniquely.

Shown in Figures E.1 and E.2 are plots of the thermal conductivity and specific heat sensitivity coefficients obtained from a Prop-1D analysis of silicon oil. The duration of experiment was 147 s, with heating at 475.15 W/m² for 90 s. From Figures E.1 and E.2 it can be seen that the sensitivity coefficients for each of the parameters are linearly independent over the range of the experiment indicating that both thermal conductivity and volumetric specific heat could be estimated individually. The sensitivity coefficients for both parameters are seen to decrease at approximately 90s, which coincides with the heat being turned off.

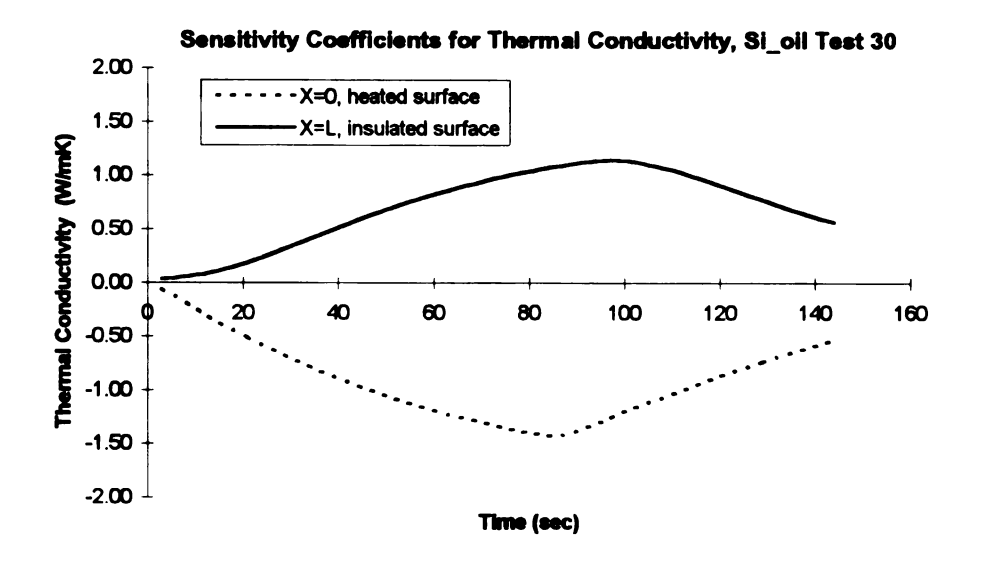


Figure E.1 Thermal conductivity sensitivity coefficients.

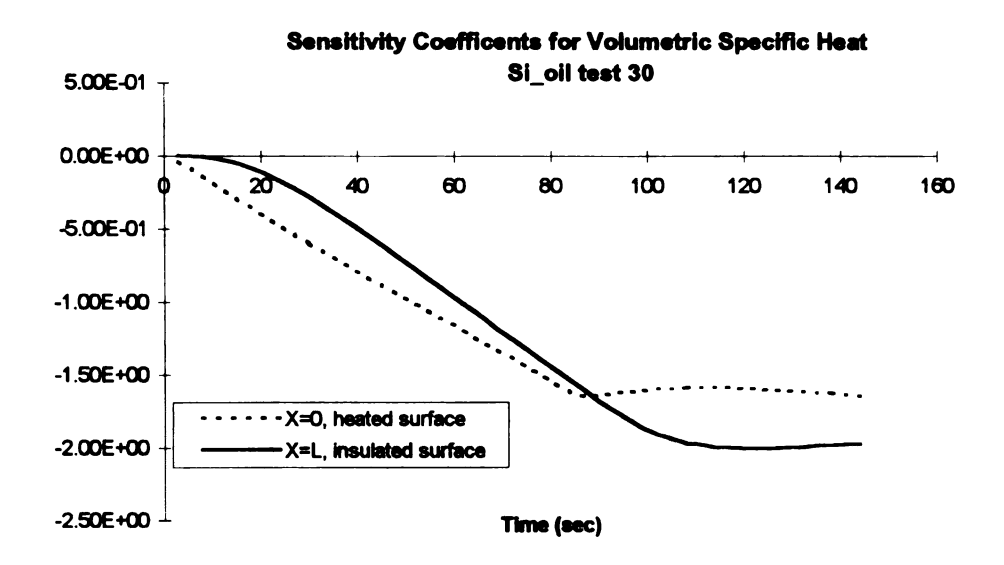


Figure E.2 Volumetric specific heat sensitivity coefficients.

Shown in Figure E.3 are the results of the Prop-1D generated temperature profiles based on the estimated parameters along with the initial experimental temperature profiles. These profiles are in good agreement.

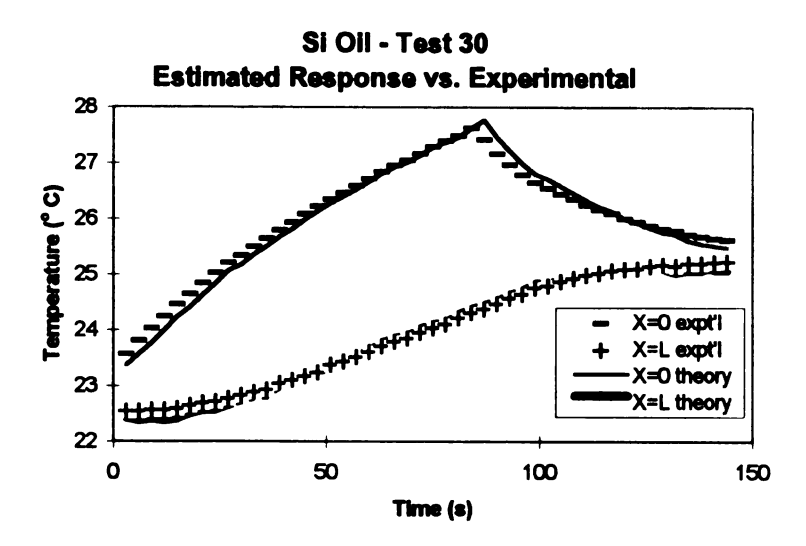


Figure E.3 Comparison of measured profiles and those generated using the parameters estimated by Prop-1D.

E.2 Sequential Estimates

Sequential estimates also provide useful information about the experiment. The sequential estimates for thermal conductivity, Figure E.4, are seen to reach a stable value and then drift down with time, indicating that perhaps 2-D effects are entering into the model at extended times. Examination of the equivalent set of sequential estimates for volumetric specific heat, Figure E.5, indicated problems with the model. Instead of reaching a steady value with increasing information, the sequential estimates looked erratic. This indicated that the model was not developed enough to accurately model the physical experiment.

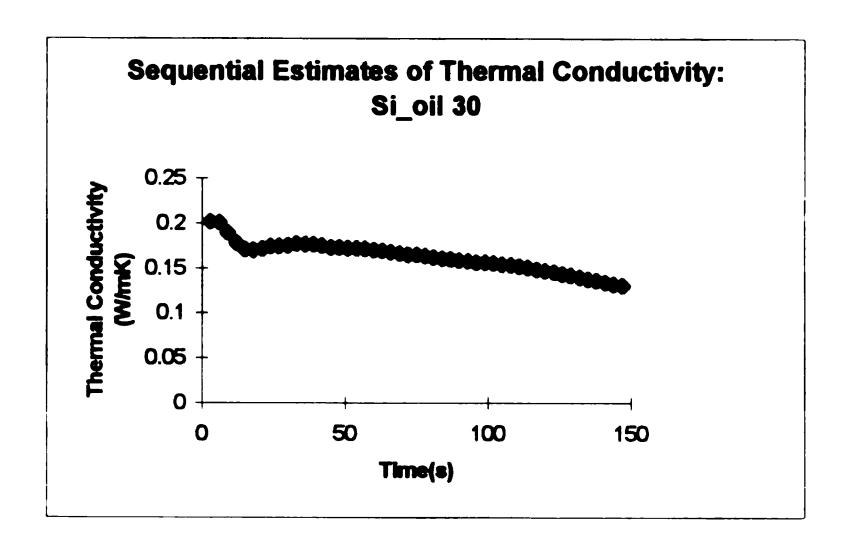


Figure E.4 Sequential estimates of thermal conductivity.

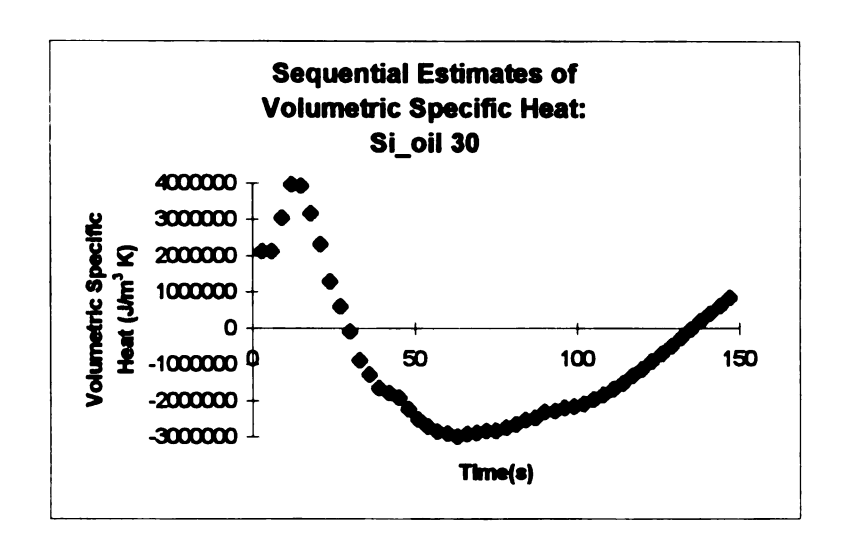


Figure E.5 Sequential estimates of volumetric specific heat.

E.3 Residuals

Residual analysis provides valuable information about the boundary conditions of the physical experiment and about the errors in the experiment in general. Shown in Figures E.6 and E.7 are the residuals for the x=0 and x=L temperature profiles. It can be seen that the residuals are highly correlated, especially at the x=0 boundary, indicating the presence of a systematic error. In both cases the residuals drift down during the last portion of the experiment, suggesting heat loss at x=L.

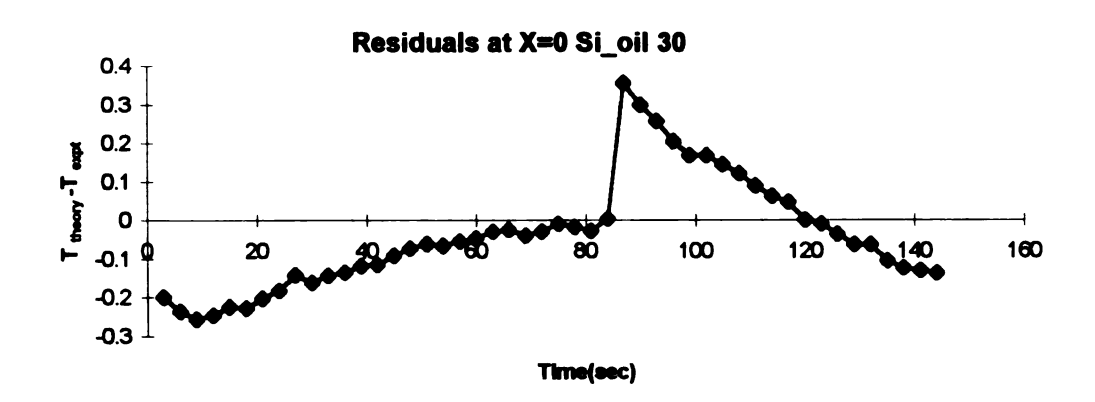


Figure E.6 Residual analysis for silicon oil, X=0 boundary.

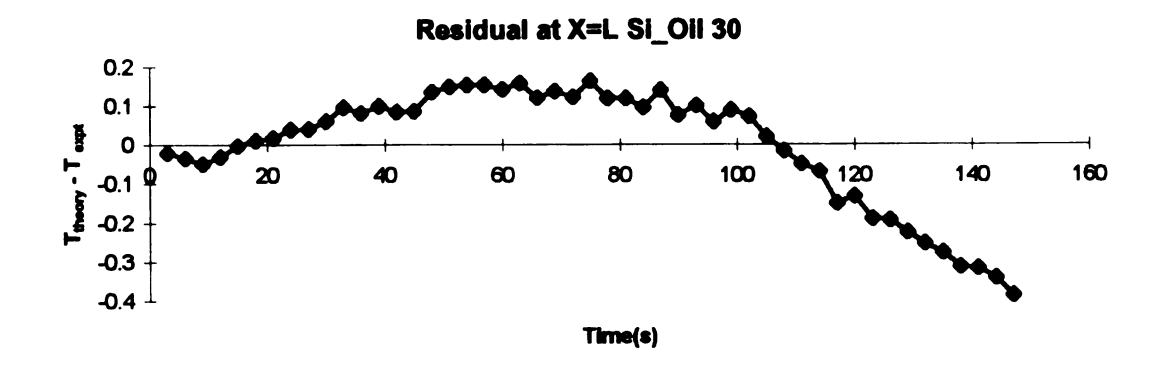


Figure E.7 Residual analysis for silicon oil, X=L boundary.

E.4 Duration of Experiment

The determination of the best duration of experiment was based on optimization of the Δ^+ criterion as outlined in Beck and Arnold (1977), for a 1-D heat conduction problem with a constant heat flux on one side and an insulated boundary condition on the other. For this case there are two optimal times, the duration of heating $(t_q^+ = 0.5)$ and the duration of experiment $(t_n^+ = 0.75)$. Depending on the thermal diffusivities of the materials tested, the optimal heating time would be different. These values are shown below in the Table E1.

	$\alpha (m^2/s)$	t _q ⁺	t _n ⁺
Silicon Oil	9.3 E-08	48.05	72.08
Water	1.44 E-07	31.10	46.65
ER fluid	6.2 E-08	72.22	108.3

Table E.1 Optimal heating and experimental duration.



Appendix F MDSC Determination of Specific Heat

F.1 Modulated Differential Scanning Calorimetry (MDSC)

Heat capacity is an extensive property characteristic of all materials and is defined as the amount of thermal energy required to raise the temperature of the specimen by 1 degree Celsius (Brady et. al, 1993). Specific heat, C_p , is the heat capacity per unit mass, and is the intensive or mass-normalized equivalent of heat capacity. It has units $J/g^{\circ}C$ or $J/kg^{\circ}K$. Heat capacity and thus specific heat are structure-sensitive properties.

Estimates of C_p for the unchained isotropic electrorheological fluid suspensions were obtained using Modulated Differential Scanning Calorimetry (MDSC). MDSC is a new technique which provides the same thermal information as conventional DSC but affords the capability to calculate a variety of other thermal transport features such as reversing and non-reversing heat flow (TA Instruments). DSC measures the heat flow difference between the analyzed material and an inert reference as a function of a linear temperature change whereas MDSC measures the difference in heat flow between the two as a simultaneous function of both a linear and a sinusoidal change in temperature. The temperature change for MDSC is given by:

$$T(t) = T_0 + \zeta t + A_T(\sin \omega t)$$
 [F.1]

where,

T(t) = Program Temperature

 T_0 = Starting Temperature

 ζ = Linear Heating Rate (°C/minute)

t = Time (minutes)

 A_T = Amplitude of Temperature Modulation (+/- °C)

 $\omega = 2\pi/P$, Modulation Frequency

P = Period(s)

The instantaneous heat flow rate is given by:

$$\frac{dq}{dt} = C_p(\beta + A_T \omega * \cos \omega t) + f'(t, T) + A_K(\sin \omega t)$$
 [F.2]

where.

 $(\beta + A_T \omega * \cos \omega t) = \text{Measured Heating Rate } (\frac{dT}{dt})$

f'(t,T) = Kinetic Response without Temperature Modulation

 $A_K =$ Amplitude of Kinetic Response to Temperature Modulation.

The total heat flow is calculated from the average value of the modulated heat flow signal and is qualitatively and quantitatively equivalent to the heat flow signal provided by conventional DSC at the same average heating rate. It represents the sum of all thermal events (melting, crystallization, etc.). C_p is determined by dividing the modulated heat flow amplitude by the modulated heating rate amplitude:

$$C_P = K(C_P) \times \left(\frac{\text{Heat Flow Amplitude(mW)}}{\text{Heating Rate Amplitude(°C/min)}}\right)$$
 [F.3]

Where DSC requires a minimum of four experimental runs, MDSC requires only two, a calibration run to determine the MDSC calibration constant and then the sample analysis. It is not necessary to run baseline profiles of empty pans.

102

The TA Instruments Thermal Analyzer was calibrated using a calibration program

included with the system's software and an indium standard, which has a well-known

melting temperature. A cell constant is calculated by the program which is used for all

subsequent tests. The MDSC cell constant was obtained using sapphire as a reference. An

MDSC run was performed using the following program:

1. Equilibriate at 5.00 °C

2. Data Storage: Off

3 Modulate +/- 1.00 °C every 60 seconds

4. Isothermal for 3.00 minutes

5. Data Storage: On

6. Ramp 5.00 °C/minute to 80.00 °C

7. Data Storage:Off

Initial Temperature: 25.00 °C 8.

Literature values of specific heat for sapphire were divided by the experimentally

obtained values to obtain values of the cell constant. The average was then used for

subsequent analyses. A second test with sapphire was run to ensure proper calibration.

Due to the difficulty associated with specific heat measurements of liquid samples, an

alternate calibration check with silicon oil was performed.

F.2 Results and Discussion

F.2.1 Calibration

The instrument's thermocouples were calibrated by using an indium standard to calculate a cell constant to be used in all subsequent tests. The previously listed MDSC program was run two times on the same 22.1 mg sapphire specimen. To determine the MDSC calibration constant the literature values of C_p at several temperatures were divided by the experimental values obtained from both runs according to:

$$K(C_p) = \frac{\text{Lit. Value}}{\text{Observed Value}}$$
 [F.4]

Table F.1 lists the results of these calculations.

Temp. (°C)	Literature	Experimental	K(C _p)	Experimental	K(C _p)
	Value	Value Specific	Run 1	Value Specific	Run 2
	Specific Heat	Heat		Heat	
	(J/g/°C)	(J/g/°C)		(J/g/°C)	
	` '	Run 1		Run 2	
16.85	0.7572	0.4828	1.5684	0.4933	1.5350
26.85	0.7788	0.5009	1.5548	0.5128	1.5187
36.85	0.7994	0.5188	1.5409	0.5322	1.5021

Table F.1 Calculation of MDSC calibration constant.

The values calculated from separate runs indicated a small degree of drift. The average of both runs, 1.5367 was inputted as the MDSC constant and used for the subsequent analyses. To ensure the adequacy of this average a third sapphire run was completed. Results indicated agreement to within 2% as indicated in table F.2.

Temp. (°C)	Experimental Cp (J/g/°C)	% Difference
16.85	0.7590	0.2377
26.85	0.7892	1.335
36.85	0.8185	2.389

Table F.2 Calibration check with sapphire.

Although sapphire is used as a general wide temperature range standard, it's composition is significantly different than the material to be analyzed, hence a run with silicon oil, the carrier fluid in the ER fluid suspensions, was performed. This material had been previously analyzed by conventional DSC and as well a literature value at a specific temperature was provided by the manufacturer. These are compared in Table F.3.

Temp. (°C)	Cp-Conventional DSC (J/g/°C)	Cp-MDSC (J/g/°C)	Cp-Literature (J/g/°C)
15.00	-	1.408	-
20.00	1.417	1.420	-
25.00	-	1.431	-
30.00	-	1.438	•
35.00	-	1.442	-
40.00	1.470	•	1.519

Table F.3 Comparison of literature and experimental values of specific heat of silicon oil.

It was found that these values were in acceptable agreement.

F.2.2 Zeolite Type 3A in Silicon Oil

The results for the ER fluids are plotted in Figure F1.

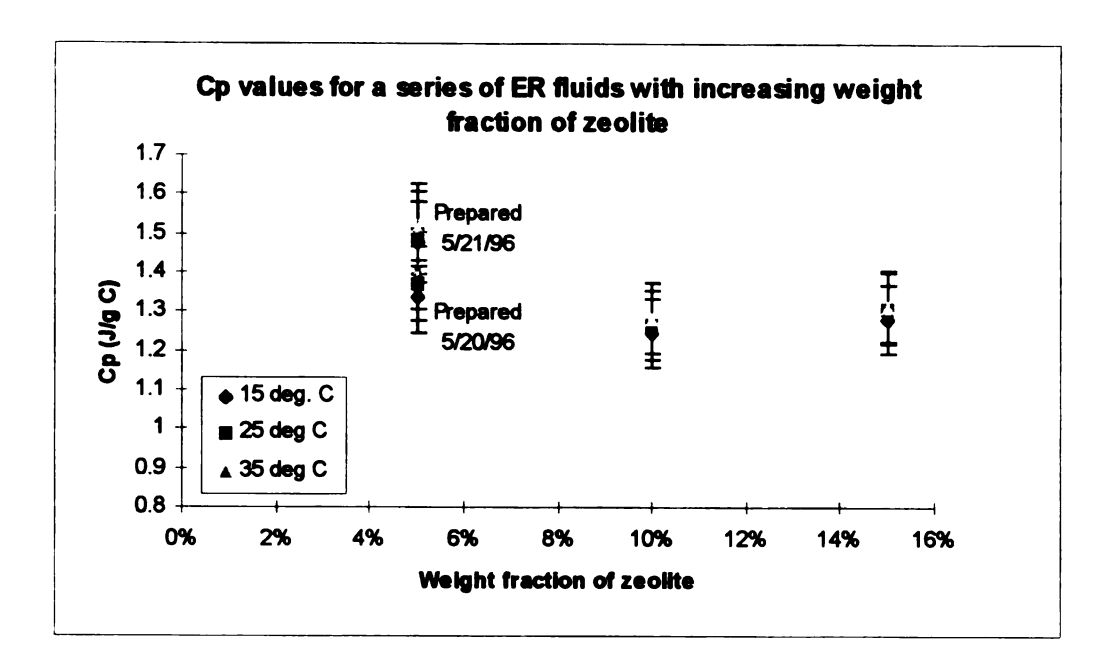


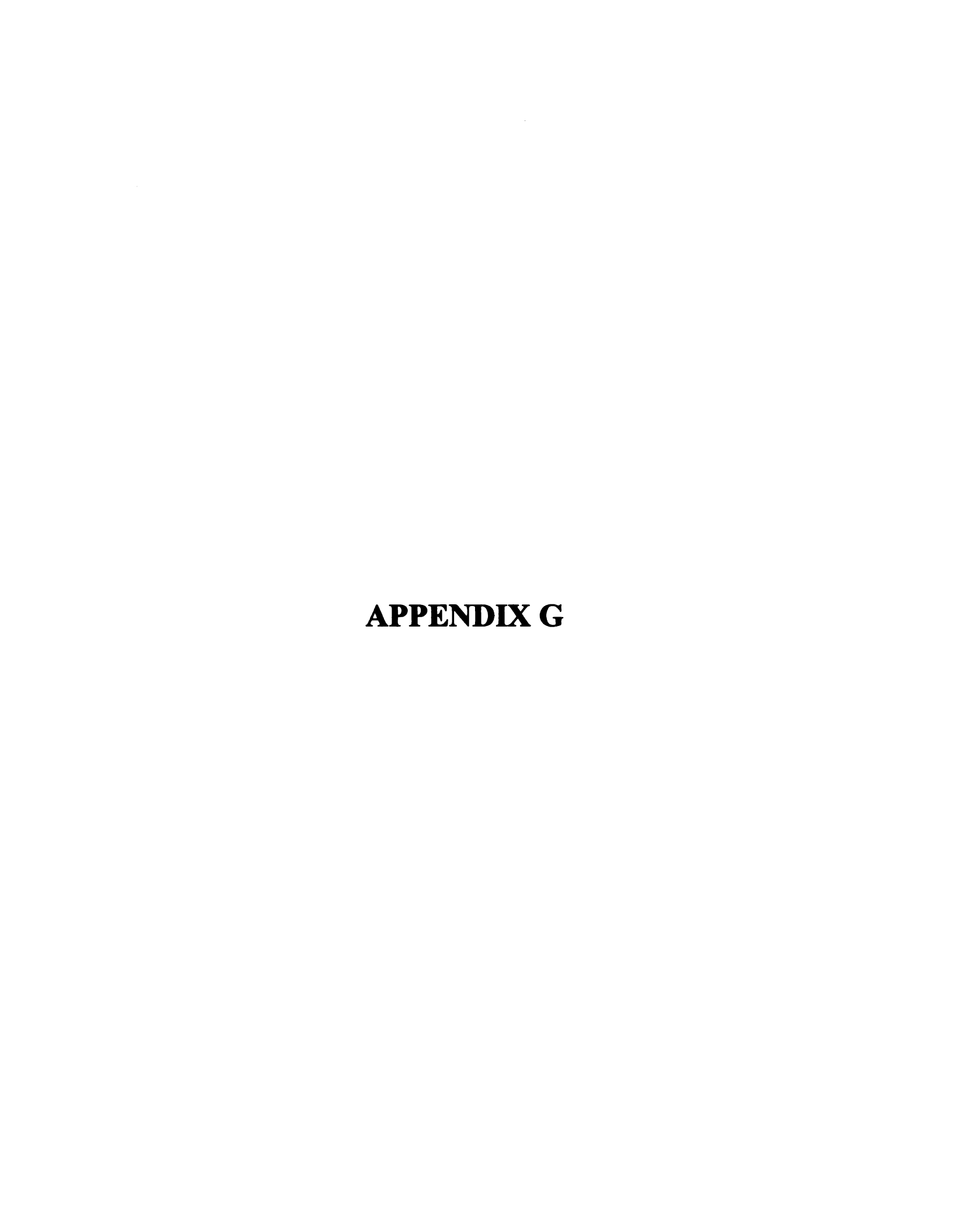
Figure F.1 Values of specific heat for a series of ER fluids.

It is interesting to note that the same fluid prepared a day later from the same base materials, but at a lower relative room humidity, gave quite different values for C_p , the wetter fluid giving a lower value of C_p . There seems to be a trend towards lower C_p values with increasing zeolite fraction. More tests would be required to substantiate this claim however.

F.2.3 Error Analysis

The above results are given with 7% error bars. There were considerable difficulties encountered when trying to obtain these measurements. The MDSC calibration constant was seen to shift around by as much as 30 % over the course of the day. To avoid such a large source of error the samples were analyzed immediately after calibration. To fully quantify the magnitude of this error it would be necessary to analyze

estimates, and observations as to trends in the C_p data should be interpreted accordingly. The 7 % error bars were chosen on the basis of the magnitude of drift in the cell constant over the course of the day (typically 15-25%), and the time required to complete the tests (roughly 3 hours). It is possible that the error bars are substantially greater than this.



Appendix G An Error and Sensitivity Analysis

The measured thicknesses of the materials used in the Prop-1D model and the associated errors are given in Table G.1

	Measured value (mm)	Error (mm)
Gasket Material	3.00	± 0.05
Aluminum	0.75	± 0.01
Heater	0.14	± 0.05
Thermal Paste	0.34	± 0.10
PVC Tape	0.16	± 0.02

Table G.1 Measurement error in material dimensions.

The duration of the experiment was known to within \pm 3 seconds, as was the duration of heating. The heat flux calculation was based on a measurement of the resistance of the heater, which was known to \pm 0.5 Ω , and the applied voltage which was known to \pm 0.05 V, and also the area of the heater which was known to \pm 0.002 cm². These measurement errors can change the heat flux by as much as 60 W/m², out of 1864 W/m².

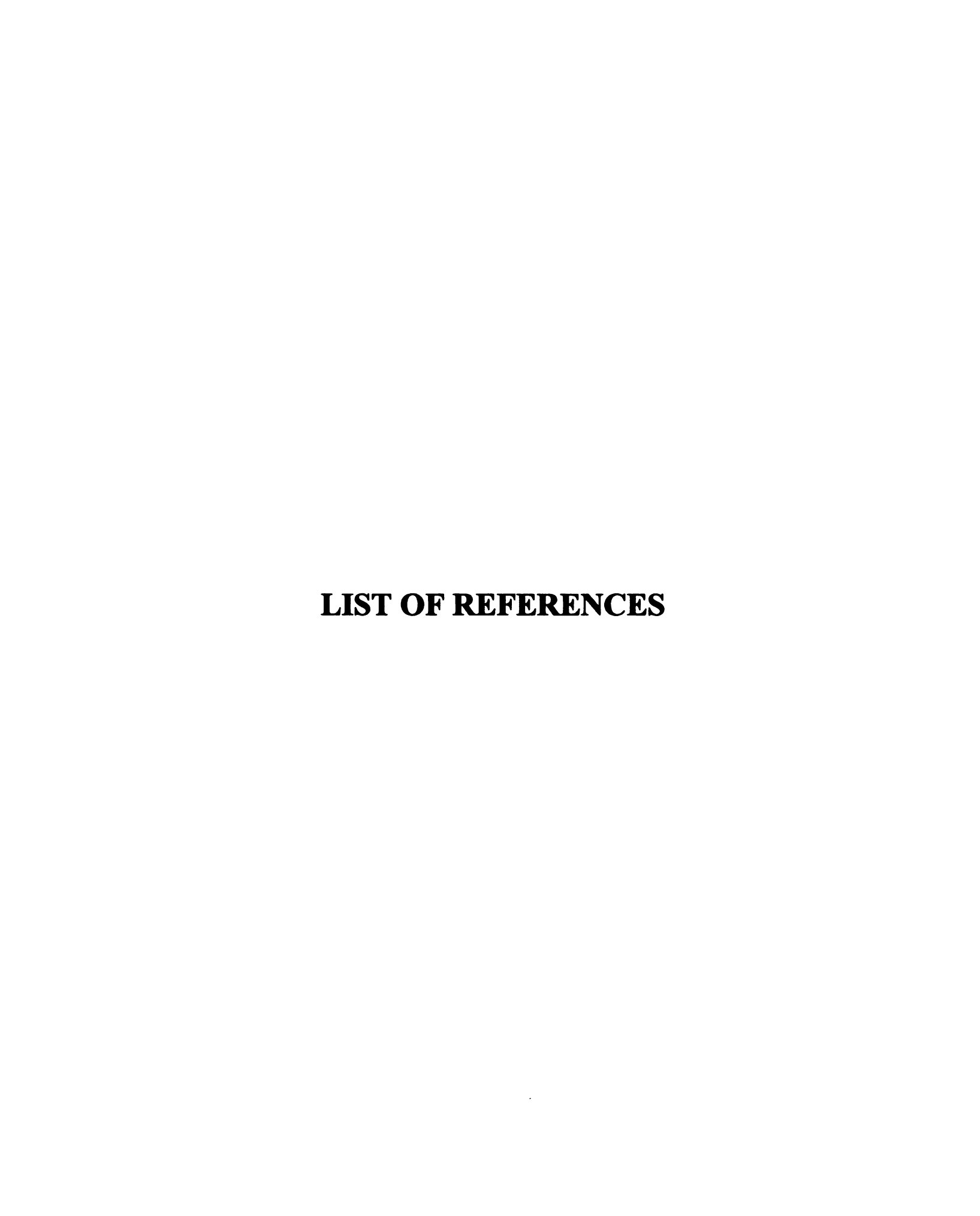
The thermal property values used in the estimation routine were primarily literature values and no estimate as to the degree of error can be given. The surface temperature as measured by the triple junction thermocouples was known to within \pm 0.2 °C.

To evaluate the sensitivity of the Prop-1D estimates to these measurement errors an estimation was performed based on a worst case scenario (all errors in one direction). The values of k and ρ Cp were re-estimated for the same ER fluid analyzed in Appendix D. The results are shown in Table G.2 along with the original estimates.

	Original Estimation	Worst Case
k	0.161 ± 0.006	0.166 ± 0.027
ρC_p	$2.3 \times 10^6 \pm 0.1 \times 10^6$	$2.2 \times 10^6 \pm 0.3 \times 10^6$

Table G.2 Sensitivity of thermal property estimation to measurement errors.

The thermal property estimates were surprisingly insensitive to measurement errors. The 95 % confidence interval was significantly larger but the generated values of k and ρC_p for the two cases did not vary greatly. This information allows k and ρC_p to be reported with confidence to \pm 0.03 and \pm 0.4 x 10⁶, respectively.



List of References

Adriani, P. M., and Gast, A.P., 1988, "A Microscopic Model of Electrorheology", *Phys. Fluids*, Vol. 31 (10)., October, pp. 2757-2768.

ASME PTC 19.3, 1974, Temperature Measurement, Part 3, Instruments and Apparatus, Supplement to ASME Performance Test Codes, p. 25.

Beck, J.V., 1962, "Calculation of Surface Heat Flux from an Internal Temperature History," ASME Paper 62-HT-46.

Beck, J.V., 1989, <u>Prop-1D Parameter Estimation Computer Program</u>, Michigan State University.

Beck, J.V., Blackwell, B., and St. Clair, Jr., C.R., 1985, <u>Inverse Heat Conduction</u>, <u>Ill-posed Problems</u>, John Wiley & Sons.

Beck, J.V., and Arnold, K.J.,1977, <u>Parameter Estimation in Engineering and Science</u>, John Wiley & Sons, New York.

Beckwith, T.J., Buck, N.L., and Marangoni, R.D., 1982, Mechanical Measurements, 3rd Ed., Addison-Wesley, Philippines, p.548.

Block, H., and Kelly, J.P., 1988, "Electrorheology", J.Phys. D:Appl. Phys., Vol. 21, p. 1661.

Boissy, C., Atten, P., and Foulc, J.-N.,1996a, "The Conduction Model of Electrorheological Effect Revisited," *Proceedings, 5th International Conference on Electrorheological Fluids, Magneto-rheological Suspensions, and Associated Technology*, W.A. Bullough, ed, World Scientific Publishing Co., Singapore, pp. 156-165.

Boissy, C., Atten, P., and Foulc, J.-N.,1996b "On the Role of Conductivities in the Electrorheological Effect," *Proceedings, 5th International Conference on Electrorheological Fluids, Magneto-rheological Suspensions, and Associated Technology,* W.A. Bullough, ed, World Scientific Publishing Co., Singapore, pp. 757-763.

Brady, J.E., and Holum, J.R., 1993, <u>Chemistry: The Study of Matter and Its Changes</u>, John Wiley & Sons, Inc., pp. 142-143, 830.

Brown, T.L., H.E. LeMay, Jr,., and B.E. Burston, 1991, <u>Chemistry, The Central Science</u>. Prentice-Hall, Inc., p. 727.

Bullough, W.A., and Stringer, J.D., 1973, "The Utilization of the Electroviscous Effect in a Fluid Power System", 3rd International Fluid Power Symposium, May 9th-11th.

Carslaw, H.S., and Jaeger, J.C., 1959, Conduction of Heat in Solids, 2nd Ed. Oxford Press University, New York.

Cha, W., D.M. Bott, and J.R. Lloyd, 1990, "Thermal Aspects of Electrorheological Fluid Based Composite Materials," Proc. American Soc. Composites, Fifth Technical Conference, East Lansing, Michigan, June 12-14, pp. 797-808.

Conrad, H., Sprecher, A.F., Choi, Y., and Chen, Y., 1991, "The Temperature Dependence of the Electrical Properties and Strength of Electrorheological Fluids", *J. Rheol.*, Vol. 35(7), pp. 1393-1410.

Conrad, H., Y.H. Shih, and Y. Chen, 1994, "Effect of Prior Heating Zeolite/Silicone Oil Suspensions on their Subsequent Rheology at 25°C", *Developments in Electrorheological Flows and Measurement Uncertainty*, ASME FED-Vol 205/AMD-Vol. 190, pp. 83-87.

Davis, L.C., 1992a, "Polarization Forces and Conductivity Effects in Electrorheological Fluids", J. Appl. Phys. 72 (4), 15 August, pp. 1334-1340.

Davis, L.C., 1992b, "Finite-Element Analysis of Particle-Particle Forces in Electrorheological Fluids", Appl. Phys. Lett. 60 (3), 20 January, pp. 319-321.

Dean, R.B., 1948, Modern Colloids, D. Van Nordstrom Company Inc., New York, p. 251.

Demchuk, S.A., Korobko, Ye. V., 1974, "Measurement of the Coefficient of Thermal Conductivity of Electrorheological Suspensions in Electric Fields," in Reofizicheskiye issledovaniya (Rheophysical Studies). Institute of Heat and Mass Transfer of the Belorussian Academy of Sciences Press, Minsk, pp. 62-67.

Duff, A.W., 1896, "The Viscosity of Polarized Dielectrics," *Physical Review*, Vol. 4, pp. 23-38.

Eige, J.J., 1963, "An Analysis of the Fluid Mechanics of Electric Fluids," ASME Paper 63-MD-1.

Everett, D.H., Ed., 1988 Basic Principles of Colloid Science, Royal Society of Chemistry,

Filisko, Frank E., 1994 "Molecular Mechanisms Associated with ER Activity: Anomolous Dispersions" FED-Vol. 205/AMD-Vol. 190, Developments in Electrorheological Flows and Measurement Uncertainty, ASME pp.1-6.

Foulc, J.-N., Atten, P., and Boissy, C., 1996, "Correlation Between Electrical and Rheological Properties of Electrorheological Fluids," *Proceedings, 5th International Conference on Electrorheological Fluids, Magneto-rheological Suspensions, and Associated Technology*, W.A. Bullough, ed, World Scientific Publishing Co., Singapore, pp. 719-726.

Furmanski, P., Floryan, J.M., 1994, "A Thermal Barrier with Adaptive Heat Transfer Characteristics," *Trans. of the ASME*, Vol. 16, May, p. 302.

Furmanski, P., Floryan, J.M., 1995, "Heat Conduction Through a Barrier Made of a Suspension of Disklike Particles," J. of Heat Transfer, Vol. 117, Aug. p. 755.

Gandhi, M.V., B.S. Thompson, and S.B. Choi, J. of Composite Materials, Vol. 23, Dec. 1989, p1282-1255

Ginder, J.M., 1993, "Diffuse Optical Probes of Particle Motion and Structure Formation in an Electrorheological Fluid," *Physical Review E*, Vol. 47(5), pp. 3418-3429.

Gebhart, B., 1993, <u>Heat Conduction and Mass Diffusion</u>, McGraw-Hill, Inc., New York, p. 589.

Graham, T., 1861, Trans. Roy. Soc. (London) 151, p.183.

Halsey, T.C., 1992, "Electrorheological Fluids," Science, Vol. 258, pp. 762-766.

Hao, T., and Xu, Y, 1996, "Dielectric Evidence for the Material Design of ER Fluids," Proceedings, 5th International Conference on Electrorheological Fluids, Magneto-rheological Suspensions, and Associated Technology, W.A. Bullough, ed, World Scientific Publishing Co., Singapore, pp. 55-63.

Harris, D.C., 1987, Quantitative Chemical Analysis, 2nd Ed., W.H. Freeman and Company, New York, pp. 416-433.

Hass, K.C., 1993, "Computer Simulations of Nonequilibrium Structure Formation in Electrorheological Fluids," *Physical Review E*, Vol. 47(5), pp. 3362-3373.

Hill, N.E., Vaughn, W.E., Price, A.H., Davies, M., (1969) <u>Dielectric Properties and Molecular Behavior</u>, Van Norstrand Reinhold Company Ltd., London

Khusid, B., and Acrivos, A., 1996, "Effects of Conductivity in Electric-Field Induced Aggregation in Electrorheological Fluids".

Kitahara, A., and Watanabe, A.,1984, "Nonaqueous systems" in Electrical Phenomena at Interfaces: Fundamentals, Measurements, and Applications, eds. A. Kitahara and A. Watanabe, pp. 119-143, Marcel Dekker, Inc., New York.

Klass, D.L., and Martinek, T.W.,1967a, "Electroviscous Fluids. I. Rheological Properties," J. of Appl. Phys., Vol. 38, No. 1, Jan., pp. 67-74.

Klass, D.L., and Martinek, T.W.,1967b, "Electroviscous Fluids. II. Electrical Properties," J. of Appl. Phys., Vol. 38, No. 1, Jan., 75-80.

Klingenberg, D.J., van Swol, F., and Zukowski, C.F., 1989, "Dynamic Simulation of Electrorheological Suspensions," J. of Chemical Physics, Vol. 91(2), pp. 7888-7895.

Kordonsky, E.V., E.V. Korobko, T.G. Lazareva, (1991) "Electrorheological Polymer-based Suspensions", J. Rheol 35(7), October, pp. 1427-1439.

Lee, S., Dulikravich, G.S., and Ahuja, V., 1993, Electro-Rheological Flows, FED-Vol.164, ASME, p.29.

Lloyd, J.R., and C. Zhang, 1994, "A Discussion on the Use of Electrorheological Fluids in the Control of Heat Transfer Processes", Proc. 1st ISHMT-ASME Heat and Mass Transfer Conference, Jan. 5-7, Bombay, India, pp. 67-77.

Makatun, V.N., Lapko, K.N., Matsepuro, A.D., and Tikavyi, V.F., 1983, "Characteristics of Charge Transport in the Disperse Phase of Electrorheological Suspensions," *Inzehenurno-Fizicheskii Zhurnal*, Vol. 45, pp. 597-602.

McGregor, K.,1997, "State Measurement and Precise Control of Electrorheological Fluids," M.S. Thesis, Michigan State University, East Lansing, MI.

Monkman, G.J., 1991, "Addition of Solid Structures to Electrorheological Fluids", J. Rheol., Vol. 35, No. 7, October, pp. 1385-1392.

Nelson, D.A., and E.C. Suydam, 1993, "The Thermal Aspects of the Electrorheological Effect and its Impact on Application Design", Electro-Rheological Flows, FED-Vol.164, ASME, p.71.

Qui, Z.Y., Hu, L., Liu, M.W., Bao, H.X., Jiang, Y.G., Zhou, L.W., Tang, Y., Gao, Z., Sun, M., and Korobko, E.V., "Temperature Effects of Dielectric Properties of ER Fluids," Proceedings, 5th International Conference on Electrorheological Fluids, Magnetorheological Suspensions, and Associated Technology, W.A. Bullough, ed, World Scientific Publishing Co., Singapore, pp. 486-493.

Quinke, G., 1897, "Viscous Behaviour of Isolated Flows in Constant Electric Fields," Annals of Physics and Chemistry, Vol. 62, pp. 1-13.

Rowe, D.M., Ed., 1995, <u>CRC Handbook of Thermoelectrics</u>, CRC Press, Boca Raton, p.166.

Schwarz, G., 1962, "A Theory of the Low-Frequency Dielectric Dipersion of Colloidal Particles in Electrolyte Solution," *J. Phys. Chem.* Vol. 66, p. 2636.

See, H., Sakurai, R., and Saito, T.,1996, "Model of Structure and Conduction in an Electrorheological Fluid Under Flow," *Proceedings, 5th International Conference on Electrorheological Fluids, Magneto-rheological Suspensions, and Associated Technology*, W.A. Bullough, ed, World Scientific Publishing Co., Singapore, pp. 478-485.

Serway, R.A., ed., 1986, <u>Physics for Scientists and Engineers with Modern Physics</u>, Sanders College Publishing, New York, pp.588-589.

Shul'man, Z.P., 1982, "Utilization of Electric and Magnetic Fields for Control of Heat and Mass Transfer in Dispersed Systems (Suspensions)," *Heat Transfer-Soviet Research*, Vol. 14(5), pp 1-23.

Shul'man, Z.P., Korobko, E.V., Matsepuro, A.D., and Khusid, B.M., 1978, "Influence of the Electroviscous Effect on Heat Transfer in the Channel between Coaxial Cylinders," *Heat Transfer - Soviet Research*, Vol. 10 (1), pp. 66-73.

Shul'man, Z.P., Matsepuro, A.D., and Khusid, B.M., 1977, "Structure Formation in Electrorheological Suspension in an Electric Field. II Quantitative," Vestsi Akad. Nauk BSSR, Ser. Fiz. -Energ. Nauk (USSR), No. 3, pp. 122-127.

Shu'lman, Z.P., Zaltsgendler, E.A., and Gleb, V.K.,1986, "Conjugated Problem of Convective Heat Transfer in Recuperative Heat Exchangers with a Non-Newtonian Heat Carrier," Int. Heat Transfer Conf., Paper MX-31, pp. 367-372.

Stangroom, J.E., 1983, "Electrorheological Fluids," Phys. Technol., Vol.14, pp. 290-296.

Stangroom, J.E., 1996, "Basic Observations on Electro-rheological Fluids," Proceedings, 5th International Conference on Electrorheological Fluids, Magneto-rheological Suspensions, and Associated Technology, W.A. Bullough, ed, World Scientific Publishing Co., Singapore, pp. 19-36.

Stolz, Jr., G., 1960, "Numerical Solutions to an Inverse Problem of Heat Conduction for Simple Shapes," J. Heat Transfer, Vol. 82, p. 20.

TA Instruments, MDSC Workshop Notes, (302)-427-4000.

Tao, R., and Sun, J.M., 1991a, "Three-Dimensional Structure of Induced Electrorheological Solid," *Physical Review Letters*, July 15th, Vol.67, No.3, pp. 398-401.

Tao, R., and Sun, J.M., 1991b, "Ground State of Electrorheological Fluids from Monte Carlo Simulations," *Physical Review Letters*, November 15th, Vol. 44, No. 6, pp. 44-47.

Uejima, H., 1972, "Dielectric Mechanism and Rheological properties of Electro-fluids," Jap. J. of Appl. Phys. 11(3), p. 319-326.

UOP Molecular Sieves Product Literature

Weiser, H.B., 1949, Colloid Chemistry, 2nd Ed., John Wiley & Sons Inc., New York, pp. 2, 227.

Whitten, K.W., Gailey, K.D., and Davis, R.E., 1992, General Chemistry, 4th Ed., Saunders College Publishing, Orlando, p.789.

Winslow, W.M., 1947, U.S. patent 2,417,850.

Winslow, W.M., 1949, "Induced Fibration of Suspensions," *Journal of Applied Physics*, Vol. 20, Dec., 1949, pp. 1137-1140.

Winslow, W.M., 1962, U.S. Patent 3,047,507.

Wu, C.W., Chen, Y., Tang, X., and Conrad, H., 1996, "Conductivity and Force Between particles in a Model Electrorheological Fluid: I Conductivity," *Proceedings, 5th International Conference on Electrorheological Fluids, Magneto-rheological Suspensions, and Associated Technology,* W.A. Bullough, ed, World Scientific Publishing Co., Singapore, pp. 525-535.

Zeng, S.Q., Hunt, A., and Greif, R., 1995, "Mean Free Path and Apparent Thermal Conductivity of a Gas in a Porous Medium", *Trans. ASME*, Vol. 117, p.758.

Zhang, C. and Lloyd, J.R., 1992, "Measurements of Radiation Heat Transfer in Electrorheological Fluid Based Composite Materials," in "Developments in Radiative Heat Transfer" HTD-Vol.203, National Heat Transfer Conference, San Diego, CA, pp. 55-62.

Zhang, C. and Lloyd, J.R., 1993, "Enhancement of Conductive Heat Transfer through an Electrorheological (ER) Fluid Based Composite Medium", 29th ASME/AIChE National Heat Transfer Conference.

Zhang, C. and Lloyd, J.R., 1994, "Control of Radiation Heat Transfer Through a Composite Window Featuring ER Fluids: A Conceptual Investigation," 2nd Minsk International Heat and Mass Transfer Forum, Minsk, Byelorussia, May 17-22, 1992.